NJC

Cite this: *New J. Chem.*, 2012, **36**, 702–722

www.rsc.org/njc

PAPER

Synthesis, limitations, and thermal properties of energetically-substituted, protonated imidazolium picrate and nitrate salts and further comparison with their methylated analogs†

Marcin Smiglak,‡[a] C. Corey Hines,[a] W. Matthew Reichert,§[a] Adam S. Vincek,[b] Alan R. Katritzky,[bc] Joseph S. Thrasher,[a] Luyi Sun,¶[a] Parker D. McCrary,[a] Preston A. Beasley,[a] Steven P. Kelley[a] and Robin D. Rogers*[a]

Received (in Gainesville, FL, USA) 4th August 2011, Accepted 6th November 2011
DOI: 10.1039/c1nj20677j

The possibility of forming simple energetic ionic liquids *via* the straightforward protonation of heterocyclic amines with nitric or picric acid was explored with 1-alkylimidazoles, 1-alkyl-2-methylimidazoles, and nitro, dinitro, and dicyano-substituted derivatives. The melting points of most of the prepared salts were lower than expected and of the 30 compounds prepared, more than half were found to melt below 100 °C. Limitations in the approach were found as a result of the use of energetic electron withdrawing substituents, such as nitro or cyano, which results in a reduction in nucleophilicity of the heterocycle and an inability to form salts with the acids studied. Interesting thermal behavior was observed with several of the new salts including supercooling and crystallization on heating. Comparison of the simple protonated imidazolium nitrate and picrate salts with their methylated analogs indicated that the protonated ionic liquids do not differ substantially in their melting points from the methylated analogs. However, the thermal stabilities of protonated imidazolium salts are much lower than their alkylated derivatives. Nitrate salts with alkylated cations tend to be more thermally stable than the corresponding picrate salts, but with protonated cations, the picrate salts tend to be approximately 70–80 °C more stable than the nitrate salts. Moreover, accelerating rate calorimetry (ARC) revealed that alkylated salts decompose much less exothermically (in some cases endothermically) than the protonated analogs, and that among all the analyzed salts, the most energetic materials found were protonated 1-methylimidazolium nitrate and 1,2-dimethylimidazolium picrate.

Introduction

Ionic liquids (ILs) are often divided into two major families based on the structure of the constituent cation: protic ionic liquids (PILs) and aprotic ionic liquids (AILs).[1,2] Using amines as an example, in PILs, the quaternary amine center is protonated as a result of the proton transfer reaction between a Brønsted acid and neutral amine, whereas in AILs, the quaternary ammonium center is fully alkylated, thus a permanent cation is created, usually as the result of the alkylation reaction of neutral amine and alkylating agent. Even though PILs are much easier to prepare in comparison to their alkylated analogs, the latter have received far greater attention over the last decade. This may be a result of the often high melting points and low thermal stabilities exhibited by PILs compared to their aprotic analogs.[2]

The existence of low melting protonated amine salts, however, is not new and can be traced back to at least an article from 1888 on the synthesis of hydroxyethylammonium nitrate, with a melting point of 52–55 °C,[3] and from 1914, a report of ethylammonium nitrate (mp 12 °C).[4] Currently, PILs are being studied for their potential in biological applications,[5,6] organic synthesis (olefin oligomerization,[7] etherification,[8] esterification,[9] and Friedel–Crafts alkylation),[10] catalysts,[11–13] chromatography,[14] proton conducting electrolytes,[15–17] and self-assembly media.[18–20]

[a] *Department of Chemistry and Center for Green Manufacturing, The University of Alabama, Box 870336, Tuscaloosa, AL 35467-0338, USA. E-mail: RDRogers@as.ua.edu*
[b] *Center for Heterocyclic Compounds, Department of Chemistry, University of Florida, Gainesville, FL 32611-7200, USA*
[c] *Department of Chemistry, King Abdulaziz University, Jeddah, Saudi Arabia*
† CCDC reference numbers 837939–837946. For crystallographic data in CIF or other electronic format see DOI: 10.1039/c1nj20677j
‡ Current Address: IoLiTec, Ionic Liquids Technologies GmbH, Satzstrasse 184, D-74076 Heilbronn, Germany.
§ Current address: Department of Chemistry, University of South Alabama, Mobile, AL 36688, USA.
¶ Current address: Department of Chemistry and Biochemistry, Texas State University-San Marcos, San Marcos, TX 78666, USA.

We have also recently proposed the use of PILs in the pharmaceutical, food, and agrichemical industries where numerous examples of active ingredients formulated as protonated salts exist.[21–23]

Limited examples of using PILs in research on energetic materials can also be found in the literature. The synthesis and characterization of protonated 1,5-diaminotetrazolium nitrate (mp 138 °C) and perchlorate (mp 97 °C) salts have been briefly described.[24] Also, the synthesis and characterization of six energetic ethylene 1,2-bis(oxyamino) nitrates, perchlorates, and dinitramides were reported, among which three (ethylene bis(oxyamine) mononitrate, ethylene bis(oxyamine) mononitramide, and ethylene bis(oxyamine) bisdinitramide) can be classified as ILs with melting points below 100 °C.[25] Recently, Gao *et al.*[26] reported the synthesis and characterization of a group of protonated ammonium and azolium salts with the 2,4,5-trinitroimidazolate anion. Utilizing simple acid–base reaction chemistry, neutral amines and azoles were paired with a very strong organic acid, 2,4,5-trinitroimidazole, resulting in formation of 17 new salts. However, only one compound in the group had a melting point below 100 °C.

Drummond and Greaves have reviewed applications of PILs in several fields,[27] however, specific literature reports focusing on systematic investigations of structure *vs*. property relationships of PILs are very limited. Examples include reports from Hirao *et al*. on heterocyclic amine-based PILs with the tetrafluoroborate anion,[28] Greaves *et al*., on primary amine-based PILs with organic carboxylate anions,[29] Luo *et al*., on thermal properties of imidazolium, ammonium, amide, and guanidine based PILs,[30,31] and Anouti *et al*., on the synthesis and physicochemical characterization of a family of alkylammonium and pyrrolidinium-based PILs.[32,33]

While the basic principles for developing and investigating protic ionic liquids are simple and well established, there exists a need to develop design criteria for the formation of ionic liquids containing energetic functional groups.[34–36] Such criteria would help to understand and predict the relationships between addition of specific energetic functional groups and the characteristics of the resultant salts. We have therefore studied protonation of a group of imidazoles containing various alkyl groups and variable substitution with common energetic nitro and cyano groups. The most straightforward, fast, and simple synthetic approach was employed for the formation of ILs *via* acid–base neutralization reactions with nitric and picric acid to form protonated azolium-based salts. Although the exact ionicity (degree of proton transfer) of the reported compounds in the liquid state is outside the scope of this work, we would refer the reader to the works of Angell,[37] MacFarlane,[38] Watanabe,[39] and even our own work[40] for a discussion of this concept and the issues it raises. Here we will focus on those aspects likely to affect practical application, the observed melting and decomposition behavior.

The targeted imidazolium-based cations were initially selected based on the substitution patterns and homological differences in the imidazole ring structures (Scheme 1). Systematic changes were implemented in the substitution patterns of N-alkyl-imidazole cores, ranging from non-energetic C-alkyl-substituted, to energetically-substituted cations (–NO_2 and –CN groups directly appended to the imidazolium core). This approach allowed for screening of a large range of products as potential EILs and subsequent determination of their properties.

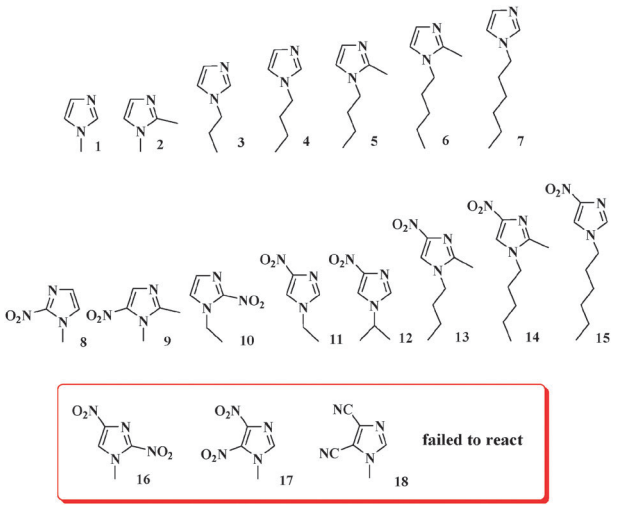

Scheme 1 Investigated imidazoles with functional groups appended to the heterocyclic core.

The main research objective addressed during our study was to develop a better understanding of relationships between structural modifications and resulting thermal properties. Specific objectives included (i) learning the influence of the electron withdrawing groups, such as –NO_2 or –CN, on the properties of the alkylimidazole ring, especially on the nucleophilicity of the nitrogen in the heterocyclic core, (ii) comparison of the thermal properties of protonated derivatives of the imidazolium cation substituted with different functional groups on the carbon positions in the heterocyclic ring (–CH_3, –NO_2, –CN), and a variety of alkyl chains on the nitrogen position of the imidazolium ring, (iii) evaluation of the influence of the chosen counterions (picrate or nitrate) on the properties of the salts and their ability to form ILs, (iv) analysis of the influence of structural changes from the protonated to methylated imidazolium salts on the thermal properties, and (v) analysis of the potential energetic character of the salts (as evaluated by self heat rate maximum values) utilizing accelerating rate calorimetry (ARC).

Results and discussion

Synthesis of N-alkylated-substituted imidazoles

Alkylimidazoles (Scheme 1) were obtained from commercial sources (**1**, **2**, **4**), previously reported literature procedures (**8–11**, **16–18**),[41] or Method A or B below. Alkylimidazoles (**3**, **7**, and **13–15**) were prepared by the alkylation of corresponding imidazoles with alkyl bromides in acetonitrile in the presence of potassium carbonate under reflux (Method A). Method A provided low isolated yields (14–44%) for products **3** and **7** likely due to the low boiling point of propyl and *iso*-propyl bromides. When the conditions were changed to potassium *tert*-butoxide in DMF at room temperature (Method B), the isolated yields of **3** and **7** improved to 72–82%. Alkylimidazoles (**5**, **6**, and **12**) were prepared by Method B.

Synthesis of protonated, substituted imidazolium nitrate or picrate salts

The syntheses of a series of protonated 1-alkylimidazoles containing combinations of nitro, cyano, or alkyl substituents were attempted (Scheme 2). The salts were prepared by neutralization reactions of the corresponding neutral azoles with nitric or picric acids in aqueous ethanol solutions. The protonated salts obtained successfully with nitrate and picrate anions include 15 cations: 1-methylimidazolium ([1-Me-3-H-IM]$^+$), 1,2-dimethylimidazolium ([1,2-diMe-3-H-IM]$^+$), 1-propylimidazolium ([1-Pr-3-H-IM]$^+$), 1-butylimidazolium ([1-Bu-3-H-IM]$^+$), 1-butyl-2-methylimidazolium ([1-Bu-2-Me-3-H-IM]$^+$), 1-pentyl-2-methylimidazolium ([1-Pent-2-Me-3-H-IM]$^+$), 1-hexylimidazolium ([1-Hex-3-H-IM]$^+$), 1-methyl-2-nitroimidazolium ([1-Me-2-NO_2-3-H-IM]$^+$), 1,2-dimethyl-5-nitroimidazolium ([1,2-diMe-5-NO_2-3-H-IM]$^+$), 1-ethyl-2-nitroimidazolium ([1-Et-2-NO_2-3-H-IM]$^+$), 1-ethyl-4-nitroimidazolium ([1-Et-4-NO_2-3-H-IM]$^+$), 1-isopropyl-4-nitroimidazolium ([1-*i*-Pr-4-NO_2-3-H-IM]$^+$), 1-butyl-2-methyl-4-nitroimidazolium ([1-Bu-2-Me-4-NO_2-3-H-IM]$^+$), 1-pentyl-2-methyl-4-nitroimidazolium ([1-Pent-2-Me-4-NO_2-3-H-IM]$^+$), and 1-hexyl-4-nitroimidazolium ([1-Hex-4-NO_2-3-H-IM]$^+$).

Limitations in the synthesis of protonated, substituted imidazolium nitrate and picrate salts

The protonation reactions utilizing 1-methyl-2,4-dinitroimidazole (**16**, 1-Me-2,4-diNO_2-IM), 1-methyl-4,5-dinitroimidazole (**17**, 1-Me-4,5-diNO_2-IM), and 1-methyl-4,5-dicyanoimidazole (**18**, 1-Me-4,5-diCN-IM) with both picric and nitric acids failed (Scheme 3). The functionalization of these heterocycles with electron-withdrawing –NO_2 or –CN substituents is thought to reduce the basicity of the heterocycle, and thus reduce its ability to form quaternary salts by protonation. These results are in agreement with the computational results presented by Gutowski *et al.*,[42] where it was concluded that the higher the electron withdrawing character of the substituents on carbon 2, 4, or 5 of the imidazole ring, the more resistant the molecule is to react with electrophiles. Furthermore, when electron withdrawing groups are added to the heterocyclic ring system, the application of stronger alkylating/protonating agents becomes necessary, and in the case of dinitro-imidazolium salts, when calculated under ideal conditions, only the triflates were reactive enough to alkylate the dinitro-imidazole precursor. We were unable to protonate these molecules even with HCl.

Further evidence of this effect was obtained from the isolation of co-crystals of 1-Me-4,5-diCN-IM and 1-Me-2,4-diNO_2-IM with picric acid (Fig. 1 and 2). This observation confirms that, due to the high electron withdrawing effect of

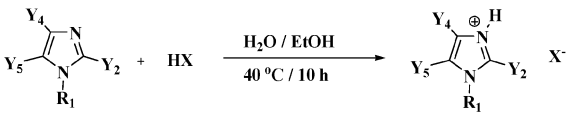

where R_1 = Alk; HX = HNO_3, $C_6H_3N_3O_7$
Y_2 = Alk, NO_2
Y_4, Y_5 = NO_2, CN

Scheme 2 General synthetic protocol for the formation of protonated substituted imidazolium nitrate and picrate salts.

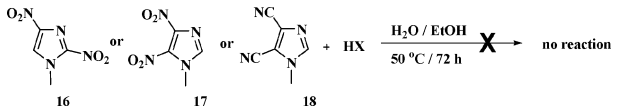

Scheme 3 Unsuccessful protonation reactions of 1-Me-2,4-diNO_2-IM (**16**), 1-Me-4,5-diNO_2-IM (**17**), and 1-Me-4,5-diCN-IM (**18**) with hydrochloric, picric, and nitric acids.

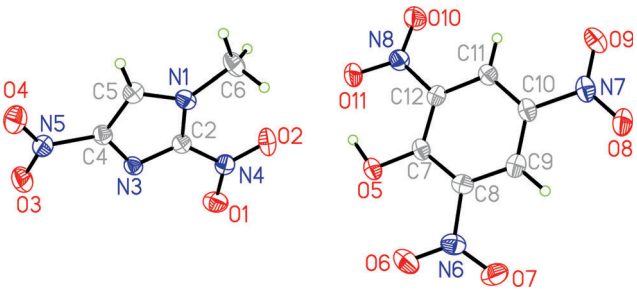

Fig. 1 50% probability ellipsoid plot of co-crystal of 1-methyl-2, 4-dinitroimidazole (16) and picric acid.

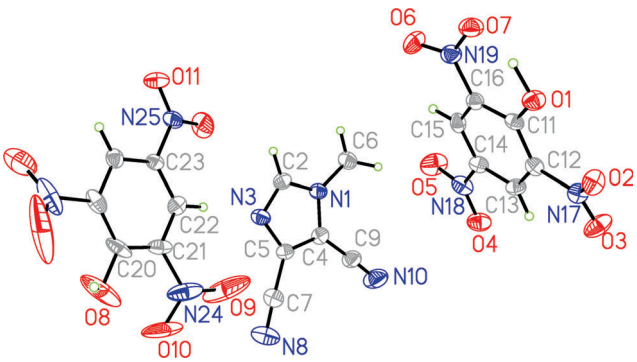

Fig. 2 50% probability ellipsoid plot of co-crystal of 1-methyl-4, 5-dicyanoimidazole (**18**) and two equivalents of picric acid.

the nitro/cyano groups attached to the imidazole core, the imidazole becomes inactive toward protonation.

Thermal investigation of protonated nitrate and picrate salts – differential scanning calorimetry analyses

Results from the DSC experiments are presented in Table 1. The results are presented such that the first data value represents the initial glass transitions for the samples which exhibit supercooled behavior after initial melting and cooling. The second value represents any liquid–liquid transitions obtained for the samples during the second and third consecutive run. Finally, the third data value represents actual melting transitions of the samples in their thermal equilibrium state. The synthesized salts varied in their thermal behavior from high melting solids, commonly observed for the highly substituted, short alkyl chain imidazolium picrate salts, to room temperature ionic liquids with glass transitions below 0 °C and no crystallization or melting transitions, as commonly observed for long alkyl chain imidazolium nitrate salts.[43] From the group of 30 compounds, more than half (23) melt below 100 °C.

Most of the crystalline salts displayed a sharp melting transition on heating, and a crystallization transition on

Table 1 Melting point transitions of the protonated substituted imidazolium salts[a]

		Thermal transitions (°C)					
Cation precursor	$[Cation]^+$	$[Picrate]^-$ (a)			$[Nitrate]^-$ (b)		
1	[1-Me-3-H-IM]$^+$	—	—	159[f] (*lit 158*)[45]	—	—	**60**[f] (*lit 70*)[46]
2	[1,2-diMe-3-H-IM]$^+$	—	—	182[f] (*lit 132*)[47]	—	—	**79**[f] (*lit 84*)[46]
3	[1-Pr-3-H-IM]$^+$	−24[b]	—	**97**[e]	−81[b]	**64**[c]	—
4	[1-Bu-3-H-IM]$^+$	−38[b]	**34**[c]	—	−76[b]	—	**6**[d]
5	[1-Bu-2-Me-3-H-IM]$^+$	—	—	104[f]	−76[b]	66[c]	—
6	[1-Pent-2-Me-3-H-IM]$^+$	—	—	127[f]	−68[b]	**48**[c]	—
7	[1-Hex-3-H-IM]$^+$	−44[b]	—	**41**[d]	−72[b]	—	**79**[d]
8	[1-Me-2-NO_2-3-H-IM]$^+$	−25[b]	38[c]	**42**[e]	—	—	**98**[f]
9	[1,2-diMe-5-NO_2-3-H-IM]$^+$	—	—	165[f]	—	—	**88**[f]
10	[1-Et-2-NO_2-3-H-IM]$^+$	−33[b]	**51**[c]	—	−60[b]	**38**[c]	—
11	[1-Et-4-NO_2-3-H-IM]$^+$	−26[b]	**42**[c]	—	−51[b]	—	**40**[f]
12	[1-*i*-Pr-4-NO_2-3-H-IM]$^+$	−28[b]	—	**57**[e]	−51[b]	**63**[c]	—
13	[1-Bu-2-Me-4-NO_2-3-H-IM]$^+$	−28[b]	**71**[c]	—	—	—	**67**[f]
14	[1-Pent-2-Me-4-NO_2-3-H-IM]$^+$	−30[b]	**67**[c]	—	—	—	**−31**[f]
15	[1-Hex-4-NO_2-3-H-IM]$^+$	−33[b]	—	**79**[d]	−63[b]	—	**11**[d]

[a] Salts meeting the definition of ILs, with melting point <100 °C, are shown in **bold**. All transitions are presented as the onset temperature for that thermal transition. [b] Glass transition (T_g) on heating, as result of initial melting and cooling of the sample, with no crystallization occurring on cooling, and formation of the glass. [c] Secondary liquid–liquid transitions (T_{l-l}). [d] Melting point of the sample (mp) where the crystallization event occurs on heating prior to the melting point. [e] Melting event occurring only during the first heating cycle (for the rest of the experiment the sample remained as a supercooled liquid). [f] Reproducible melting point.

cooling from the melt. However, several of the lower melting salts only crystallized slowly on heating after their initial melting, cooling, and glass transitions. The melting transitions of many of the salts were poorly defined in the DSC, commonly having a characteristic broad transition with a strong leading edge.

Only a few of the analyzed salts exhibited simple thermal behavior with a sharp melting point on heating and subsequent crystallization on cooling that were reproducible throughout all heating and cooling cycles, and, interestingly, none of those salts exhibited glass transitions (Fig. 3, Example **A**). These samples include: [1-Me-3-H-IM][Pic] (**1a**), [1,2-diMe-3-H-IM][Pic] (**2a**), [1-Bu-2-Me-3-H-IM][Pic] (**5a**), [1-Pent-2-Me-3-H-IM][Pic] (**6a**), [1,2-diMe-5-NO_2-3-H-IM][Pic] (**9a**), [1-Me-3-H-IM][NO_3] (**1b**), [1,2-diMe-3-H-IM][NO_3] (**2b**), [1-Me-2-NO_2-3-H-IM][NO_3] (**8b**), [1,2-diMe-5-NO_2-3-H-IM][NO_3] (**9b**), [1-Bu-2-Me-4-NO_2-3-H-IM][NO_3] (**13b**), and [1-Pent-2-Me-4-NO_2-3-H-IM][NO_3] (**14b**).

All other salts exhibited more complicated thermal behavior and can be divided into three groups. The first group includes the compounds that, during the first heating cycle, exhibited a melting point transition, but no crystallization was observed during the cooling cycle, leading to the formation of a glass as a result of supercooled behavior. Those supercooled salts, upon heating and after passing the glass transition, undergo (i) crystallization transition just prior to the expected melting point and (ii) melting transition in the expected temperature range. Compounds exhibiting such thermal characteristics include: [1-Hex-3-H-IM][Pic] (**7a**), [1-Hex-4-NO_2-3-H-IM][Pic] (**15a**), [1-Bu-3-H-IM][NO_3] (**4b**), [1-Hex-3-H-IM][NO_3] (**7b**), and [1-Hex-4-NO_2-3-H-IM][NO_3] (**15b**) (Fig. 3, Example **B**).

The second group includes the compounds that exhibited a melting point only during their first heating cycle, after which the salts exhibited supercooled characteristics with no crystallization on cooling, a glass transition on cooling and on heating, and neither crystallization nor melting during consecutive cycles. Those salts include: [1-Pr-3-H-IM][Pic] (**3a**) and [1-*i*-Pr-4-NO_2-3-H-IM][Pic] (**12a**).

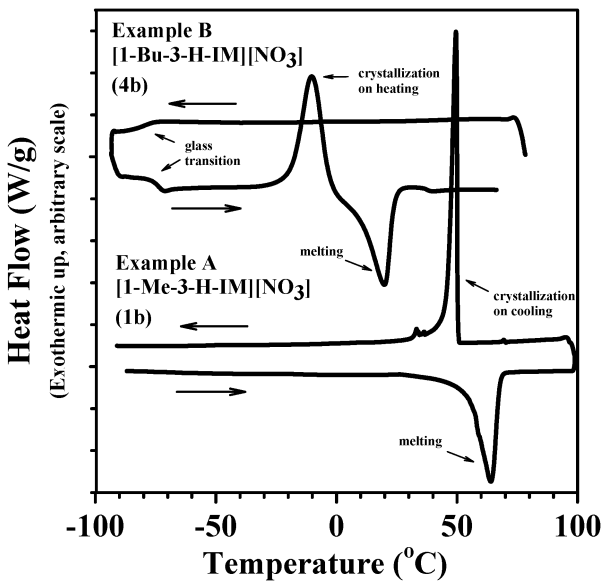

Fig. 3 Characteristic thermal behavior of examples: Example **A** – typical thermal behavior with a melting transition on heating and crystallization on cooling; Example **B** – supercooled behavior with initial melting of the sample (mp), and cooling with no crystallization follow by glass transition (T_g), crystallization, and melting on heating.

The last group of compounds includes the salts that exhibited rather unusual thermal behavior. They showed (i) difficult to define broad transitions on heating, (ii) no crystallization transitions on cooling, (iii) glass transitions on cooling and heating, (iv) no crystallization or melting on heating, but only (v) liquid–liquid transitions above room temperature that resemble secondary glass transitions. Samples exhibiting this kind of thermal behavior include: [1-Bu-3-H-IM][Pic] (**4a**),

[1-Me-2-NO_2-3-H-IM][Pic] (**8a**), [1-Et-2-NO_2-3-H-IM][Pic] (**10a**), [1-Et-4-NO_2-3-H-IM][Pic] (**11a**), [1-Bu-2-Me-4-NO_2-3-H-IM][Pic] (**13a**), [1-Pent-2-Me-4-NO_2-3-H-IM][Pic] (**14a**), [1-Pr-3-H-IM][NO_3] (**3b**), [1-Bu-2-Me-3-H-IM][NO_3] (**5b**), [1-Pent-2-Me-3-H-IM][NO_3] (**6b**), [1-Et-2-NO_2-3-H-IM][NO_3] (**10b**), [1-Et-4-NO_2-3-H-IM][NO_3] (**11b**), and [1-*i*-Pr-4-NO_2-3-H-IM][NO_3] (**12b**).

The characteristic DSC traces of this group of salts showed a real glass transition below 0 °C, then a second glass-like transition above room temperature during the second and third DSC cycles. It was noted that the secondary transitions occurred closely, with much reduced intensity, to expected crystallization and melting transitions. The thermal transitions of the above mentioned salts, described as liquid–liquid transitions, appear to be the temperatures of crystallization of the particular salts, but because of their slow crystallization processes, the actual crystallization does not occur and only something appearing like a secondary glass transition is recorded. To support the argument that the observed liquid–liquid transitions are real attempts of the sample to crystallize and melt, the below two examples are presented (Fig. 4 and 5).

Fig. 4 presents a comparison of the second cycles of DSC scans for [1-Hex-4-NO_2-3-H-IM][Pic] (**15a**) (mp = 79 °C) (Example **A**), [1-Hex-3-H-IM][Pic] (**7a**) (mp = 41 °C) (Example **B**), and [1-Bu-2-Me-4-NO_2-3-H-IM][Pic] (**13a**) ($T_{l\text{–}l}$ = 71 °C) (Example **C**). All of the samples exhibit glass transitions below room temperature as the result of their supercooled behavior. For [1-Hex-4-NO_2-3-H-IM][Pic] (**15a**), after initial melting during the first heating cycle the sample does not crystallize on cooling but undergoes a glass transition and subsequent crystallization and melting on heating only. [1-Hex-3-H-IM][Pic] (**7a**) exhibits a similar shape in the DSC trace to [1-Hex-4-NO_2-3-H-IM][Pic] (**15a**) in the melting region, but the crystallization/melting trace is much reduced in intensity. The same is observed for the [1-Bu-2-Me-4-NO_2-3-H-IM][Pic] (**13a**), where in the region suspected of exhibiting melting behavior the crystallization/melting does not occur and only a $T_{l\text{–}l}$ is observed. Based on the structural difference between

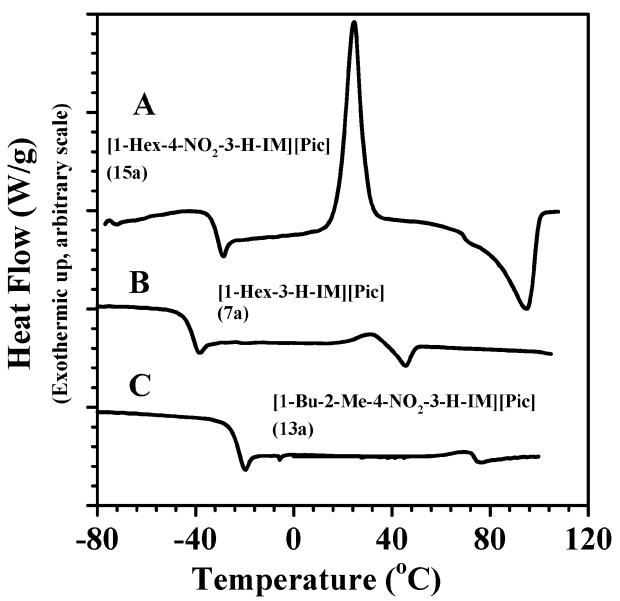

Fig. 4 Comparison of exemplary DSC traces of supercooled behavior. The DSC traces are shown for the second heating cycle.

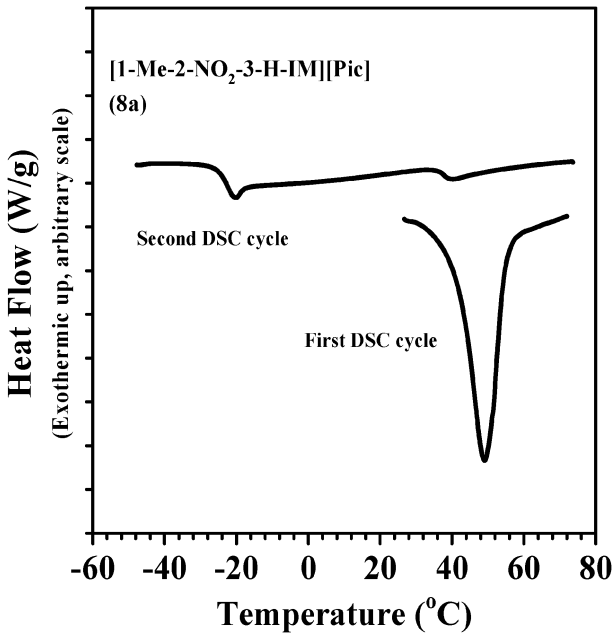

Fig. 5 DSC traces of [1-Me-2-NO_2-3-H-IM][Pic] (**8a**) showing a sharp melting point on heating (during the first heating cycle) and a glass transition and liquid–liquid transition (during the second heating cycle) as a result of supercooled behavior.

[1-Hex-3-H-IM][Pic] (**7a**) and [1-Hex-4-NO_2-3-H-IM][Pic] (**15a**), it was expected that **7a** would exhibit a lower melting point than **15a**, due to the absence of the additional substituent in the imidazolium ring, which usually tends to cause an increase in the melting point of those salts. The difference in the melting points between those two compounds was not, however, expected to be very large.

Another example, the thermogram of [1-Me-2-NO_2-3-H-IM][Pic] (**8a**) (Fig. 5) clearly shows that the sample after an initial melting transition at 42 °C, and consecutive cooling, did not crystallize but instead exhibited supercooled characteristics, with a glass transition at −25 °C. When heated for the second time, neither crystallization nor melting transitions were observed; however, a liquid–liquid transition was seen in the temperature region previously recognized as a melting point transition. Furthermore, after the sample was left for a one week period in a closed vial and then DSC analyses performed again, the sample exhibited a melting point during the first heating cycle in the region as observed previously and no crystallization or melting transitions in any of the consecutive runs. As a result, it was decided to consider the observed secondary $T_{l\text{–}l}$ transitions as attempts of the salt to crystallize; thus we have decided to treat these liquid–liquid transitions as indications of the melting points of the analyzed samples. Such assumptions allow for better comparisons of melting points of the salts and aids in drawing conclusions regarding the observed trends in melting points.

As expected, the general trends in the melting points of the salts show that melting transitions of picrate-based salts are always higher than that of their nitrate equivalents. Picrate-based salts exhibit melting points ranging from 182 °C for [1,2-diMe-3-H-IM][Pic] (**2a**) to 34 °C for [1-Bu-3-H-IM][Pic] (**4a**) (recognized as a liquid–liquid transition). On the other hand, the melting points of nitrate-based salts range from 98 °C for

[1-Me-2-NO_2-3-H-IM][NO_3] (**8b**) to 6 °C for [1-Bu-3-H-IM][NO_3] (**4b**).

Analyzing the melting point variation as a function of the *N*-alkyl chain length, it was noted that the longer the alkyl chain, the lower the melting point of the resulting salts, until the alkyl chain extends over four carbons, at which point an increase of the melting point is observed in most cases. This behaviour is not uncommon among other ILs, and it is often observed that the melting point minimum for alkylimidazolium-based salts ranges between three and six carbons in the alkyl chain, after which the melting point starts to increase.[44] The melting points of the 1-alkylimidazolium picrate salts follow the trend: 159 °C for [1-Me-3-H-IM]$^+$ (**1a**), 97 °C for [1-Pr-3-H-IM]$^+$ (**3a**), 34 °C for [1-Bu-3-H-IM]$^+$ (**4a**), and 41 °C for [1-Hex-3-H-IM]$^+$ (**7a**). A similar trend is observed for 1-alkylimidazolium nitrate salts: 60 °C for [1-Me-3-H-IM]$^+$ (**1b**), 64 °C for [1-Pr-3-H-IM]$^+$ (**3b**), 6 °C for [1-Bu-3-H-IM]$^+$ (**4b**), and 79 °C for [1-Hex-3-H-IM]$^+$ (**7b**).

Analysis of the structure *vs.* melting point relationships between different 1-alkyl-2-methyl-4 (or 5)-nitro-substituted imidazolium salts reveals a similar trend to the 1-alkylimidazolium salts, where the longer the *N*-alkyl chain-substituted on the nitrogen position, the lower the melting point of the resulting salt. The replacement of the C2-H position with a methyl group did not influence this trend. For both picrate and nitrate salts the expected trend is easily recognizable; for picrates: 165 °C for [1,2-diMe-5-NO_2-3-H-IM]$^+$ (**9a**), 71 °C for [1-Bu-2-Me-4-NO_2-3-H-IM]$^+$ (**13a**), and 67 °C for [1-Pent-2-Me-4-NO_2-3-H-IM]$^+$ (**14a**); and for nitrates: 88 °C for [1,2-diMe-5-NO_2-3-H-IM]$^+$ (**9b**), 67 °C for [1-Bu-2-Me-4-NO_2-3-H-IM]$^+$ (**13b**), and −31 °C for [1-Pent-2-Me-4-NO_2-3-H-IM]$^+$ (**14b**). Such behavior has also been reported previously.[44]

Further analysis of the influence of the cation structure on the melting points of the obtained salts revealed that 1,2-dialkyl-substituted salts melt at higher temperatures than those not possessing the methyl substituent on the C2 carbon position in the ring; 182 °C *vs.* 159 °C for [1,2-diMe-3-H-IM][Pic] (**2a**) *vs.* [1-Me-3-H-IM][Pic] (**1a**), 79 °C *vs.* 60 °C for [1,2-diMe-3-H-IM][NO_3] (**2b**) *vs.* [1-Me-3-H-IM][NO_3] (**1b**), 104 °C *vs.* 34 °C for [1-Bu-2-Me-3-H-IM][Pic] (**5a**) *vs.* [1-Bu-3-H-IM][Pic] (**4a**), and 66 °C *vs.* 6 °C for [1-Bu-2-Me-3-H-IM][NO_3] (**5b**) *vs.* [1-Bu-3-H-IM][NO_3] (**4b**).

To compare the influence of the position of the –NO_2 group on the melting point of the salts, two isomeric cations were prepared, where the only difference between them was the position of the –NO_2 group on the heterocyclic ring. In the case of [1-Et-2-NO_2-3-H-IM][NO_3] (**10b**) (mp 38 °C) and [1-Et-4-NO_2-3-H-IM][NO_3] (**11b**) (mp 40 °C), the melting point difference is 2 °C, and in the case of [1-Et-2-NO_2-3-H-IM][Pic] (**10a**) (mp 51 °C) and [1-Et-4-NO_2-3-H-IM][Pic] (**11a**) (mp 42 °C) this difference is 9 °C. Based on this finding it was concluded that the position of the –NO_2 substituent does not have any substantial influence on the melting point of the formed salt, but as it will be shown later, it does have substantial effect on the thermal stabilities of the analyzed salts.

Thermal investigation of protonated nitrate and picrate salts–thermogravimetric analyses

Table 2 records the onset temperatures for 5% decomposition ($T_{5\%dec}$) as obtained by TGA analyses of the salts. Variations of their thermal stabilities were observed depending on the structural characteristics of the cation, as well as on the anion used, ranging in decomposition temperatures from 226 °C to 69 °C. Most of the investigated salts exhibited simple thermal decomposition behavior with a single decomposition step. The exceptions from this behavior were evident in three examples of nitro-substituted imidazolium nitrate salts: [1-Bu-2-Me-4-NO_2-3-H-IM][NO_3] (**13b**), [1-Pent-2-Me-4-NO_2-3-H-IM][NO_3] (**14b**), and [1-Hex-4-NO_2-3-H-IM][NO_3] (**15b**).

Table 2 Thermal stabilities[a]

Cation precursor	Cation	Thermal stabilities (°C)	
		Picrates (a)	Nitrates (b)
1	[1-Me-3-H-IM]$^+$	184	137
2	[1,2-diMe-3-H-IM]$^+$	209	131
3	[1-Pr-3-H-IM]$^+$	177	143
4	[1-Bu-3-H-IM]$^+$	198	150
5	[1-Bu-2-Me-3-H-IM]$^+$	224	121
6	[1-Pent-2-Me-3-H-IM]$^+$	226	137
7	[1-Hex-3-H-IM]$^+$	188	138
8	[1-Me-2-NO_2-3-H-IM]$^+$	112	82
9	[1,2-diMe-5-NO_2-3-H-IM]$^+$	145	123
10	[1-Et-2-NO_2-3-H-IM]$^+$	107	69
11	[1-Et-4-NO_2-3-H-IM]$^+$	157	83, 141[b]
12	[1-*i*-Pr-4-NO_2-3-H-IM]$^+$	137	87, 192[b]
13	[1-Bu-2-Me-4-NO_2-3-H-IM]$^+$	188	102, 213[b]
14	[1-Pent-2-Me-4-NO_2-3-H-IM]$^+$	176	104, 203[b]
15	[1-Hex-4-NO_2-3-H-IM]$^+$	175	102, 231[b]

[a] All transitions are presented as the onset temperature for the 5% decomposition ($T_{5\%dec}$). [b] Sample with two distinguishable decomposition slopes; the given value is the onset temperature for the second decomposition step.

Generally, the analyzed imidazolium picrate salts decomposed in the thermal range between 226 °C ([1-Pent-2-Me-3-H-IM][Pic] (**6a**)) and 107 °C ([1-Et-2-NO_2-3-H-IM][Pic] (**10a**)). The thermal stabilities of the analogous nitrate salts varied from 150 °C ([1-Bu-3-H-IM][NO_3] (**4b**)) to 69 °C ([1-Et-2-NO_2-3-H-IM][NO_3] (**10b**)). Examination of data indicates that the thermal stabilities of all nitrate-based salts are lower than that of their picrate-based analogs. Typically, the difference between the thermal stabilities of nitrate and picrate salts was *ca.* 50 °C, but in some cases varied between 20 and 100 °C. Moreover, it was noticed that all unsubstituted imidazolium salts exhibited higher stabilities of *ca.* 50 °C, compared to any mononitro-substituted salts.

Comparison of the thermal stabilities of protonated, non-nitro-substituted imidazolium picrate and nitrate salts

All non-nitro-substituted imidazolium salts exhibit simple decomposition characteristics with single-step decomposition. The $T_{5\%dec}$ values for the picrate salts vary between 177 °C for [1-Pr-3-H-IM][Pic] (**3a**) and 226 °C for [1-Pent-2-Me-3-H-IM][Pic] (**6a**). For the nitrate analogs, they do not vary substantially, with onset temperatures between 121 °C for [1-Bu-2-Me-3-H-IM][NO_3] (**5b**) and 150 °C for [1-Bu-3-H-IM][NO_3] (**4b**). Comparing the homologous series of compounds [1-Me; 1-Pr; 1-Bu; 1-Hex-3-H-IM][Pic], the decomposition temperatures do not seem to have any correlation with alkyl chain length, with $T_{5\%dec}$ of 177 °C (1-Pr) < 184 °C (1-Me) < 188 °C (1-Hex) < 198 °C (1-Bu). Comparing the nitrate equivalents of the same group of cations, it was noted that

all of those salts decomposed in a very narrow temperature range, and in fact, the maximum difference between $T_{5\%dec}$ is 13 °C: 137 °C (1-Me) < 138 °C (1-Hex) < 143 °C (1-Pr) < 150 °C (1-Bu).

When considering compounds with a methyl substituent on the C2 position of the ring, a noticeable trend arises for the picrate salts. The C2-Me-substituted salts exhibit higher decomposition temperatures (*ca.* 20 °C) than those that are unsubstituted at the C2 carbon. Comparing [1-Me-3-H-IM][Pic] (**1a**) to [1,2-diMe-3-H-IM][Pic] (**2a**), the $T_{5\%dec}$ increased from 184 °C to 209 °C and from [1-Bu-3-H-IM][Pic] (**4a**) to [1-Bu-2-Me-3-H-IM][Pic] (**5a**), the $T_{5\%dec}$ increased from 198 °C to 224 °C. Additionally, it was noted that the decomposition temperatures of C2-Me-substituted picrate salts increased slightly as the alkyl chain length increased; from 209 °C (1,2-diMe-substituted) to 224 °C (1-Bu-2-Me-substituted) to 226 °C (1-Pent-2-Me-substituted). Interestingly, the C2-Me-substituted nitrate salts exhibit lower decomposition temperatures than the unsubstituted analogs; 137 °C $[1\text{-Me-3-H-IM}]^+$ (**1b**) > 131 °C $[1,2\text{-diMe-3-H-IM}]^+$ (**2b**) and 150 °C $[1\text{-Bu-3-H-IM}]^+$ (**4b**) > 121 °C $[1\text{-Bu-2-Me-3-H-IM}]^+$ (**5b**). Moreover, changing the length of the *N*-alkyl chain in the C2-Me-substituted 1-alkylimidazolium nitrates does not seem to significantly influence the decomposition temperature of the resulting salt: 131 °C (1,2-diMe-substituted), 121 °C (1-Bu-2-Me-substituted), and 137 °C (1-Pent-2-Me-substituted).

From these results it could be concluded that protonated, non-nitro-substituted imidazolium picrate salts are more thermally stable than their nitrate salt equivalents, and that the C2-Me-substituted picrate salts tend to be more stable than those which are unsubstituted, however, they also have higher melting points. It was also concluded that the thermal stability range for each group of salts is more dependent on the structure of the anion than on the presence of substituents on the C2 carbon or the alkyl chain length of the *N*-alkyl substituents.

Thermal stabilities of protonated, nitro-substituted imidazolium picrate and nitrate salts

The $T_{5\%dec}$ decomposition temperatures for these picrate salts vary between 107 °C for [1-Et-2-NO_2-3-H-IM][Pic] (**10a**) and 188 °C for [1-Bu-2-Me-3-H-4-NO_2-IM][Pic] (**13a**). For the nitrates $T_{5\%dec}$ vary less from each other, with $T_{5\%dec}$ between 69 °C for [1-Et-2-NO_2-3-H-IM][NO_3] (**10b**)) and 123 °C for [1,2-diMe-5-NO_2-3-H-IM][NO_3] (**9b**). Generally, the decomposition temperatures for the nitrate and picrate salts of the –NO_2-substituted alkylimidazoles seems to be *ca.* 20–50 °C lower than of those not substituted with nitro groups. Increasing the length of the alkyl chain on the nitrogen seems to cause a slight decrease in the thermal stability of the nitro-substituted imidazolium salts. This can be seen in the example of both picrates (112 °C *vs.* 107 °C), albeit less clear a difference than in the nitrates, (82 °C *vs.* 69 °C) of $[1\text{-Me-2-NO}_2\text{-3-H-IM}]^+$ and $[1\text{-Et-2-NO}_2\text{-3-H-IM}]^+$ cation-based salts.

Next, it was noticed that by changing the position of the –NO_2 substituent from the C2 to the C4 carbon in the imidazolium ring, an increase in the stability of the resulting salt was observed for both picrates and nitrates. The $T_{5\%dec}$ of [1-Et-2-NO_2-3-H-IM][Pic] (**10a**) and $[NO_3]^-$ (**10b**) are 107 °C and 69 °C, respectively while for [1-Et-4-NO_2-3-H-IM][Pic] (**11a**) and $[NO_3]^-$ (**11b**) they are 157 °C and 83 °C, respectively. In contrast, the melting points for those pairs of compounds remained similar (with a maximum difference of <10 °C). The substitution of the C2 carbon position with a –NO_2 group in comparison to a –Me group resulted in a decrease of stability in the picrate salts from 209 °C ($[1,2\text{-diMe-3-H-IM}]^+$ (**2a**)) to 112 °C ($[1\text{-Me-2-NO}_2\text{-3-H-IM}]^+$ (**8a**)), as well as in the case of nitrate analogs, 131 °C ($[1,2\text{-diMe-3-H-IM}]^+$ (**2b**)) to 82 °C ($[1\text{-Me-2-NO}_2\text{-3-H-IM}]^+$ (**8b**)).

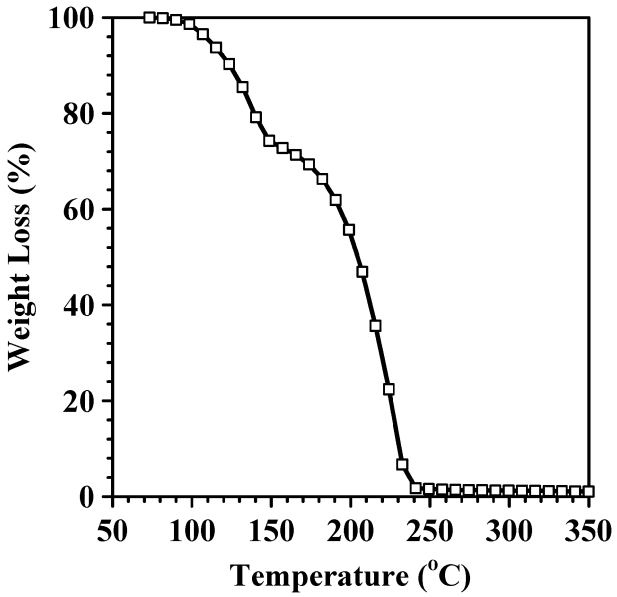

Fig. 6 Characteristic two step decomposition processes observed for 4-NO_2-substituted alkylimidazolium nitrates ([1-Pent-2-Me-4-NO_2-3-H-IM][NO_3] (**14b**) shown).

When considering all 4-NO_2-substituted alkylimidazolium nitrates, two separate decomposition steps were observed. The first occurs at *ca.* 100 °C and ends at *ca.* 150 °C, while the second starts between *ca.* 180 °C and 200 °C. The loss of weight during the first decomposition step (*ca.* 18–28 wt%) seems to match the loss of an HNO_3 molecule as the result of a deprotonation reaction and evacuation of the acid from the system (Fig. 6). This deprotonation and subsequent evaporation of the acid would lead to the formation of the starting amine and its evaporation at *ca.* 200 °C. Such two-step decomposition was not seen for any other salt with an *N*-alkyl chain shorter than ethyl, and it was not observed for any of the non-nitro-substituted salts.

Syntheses of selected alkylated imidazolium nitrate and picrate salts and thermal analysis for comparison with protonated analogs

Methyl-alkylated analogs of a series of nitrate and picrate salts were also prepared in order to compare the thermal behavior of families of protonated *vs.* alkylated salts (Scheme 4). The compounds included 1,3-dimethylimidazolium picrate ([1,3-diMeIM][Pic]) (**19a**), 1,2,3-trimethylimidazolium picrate ([1,2,3-triMeIM][Pic]) (**20a**), 1-butyl-3-methylimdazolium picrate ([1-Bu-3-MeIM][Pic]) (**21a**), 1,3-dimethylimidazolium nitrate ([1,3-diMeIM][NO_3]) (**19b**), 1,2,3-trimethylimidazolium nitrate ([1,2,3-triMeIM][NO_3]) (**20b**), and 1-butyl-3-methyl-imidazolium nitrate ([1-Bu-3-MeIM][NO_3]) (**21b**).

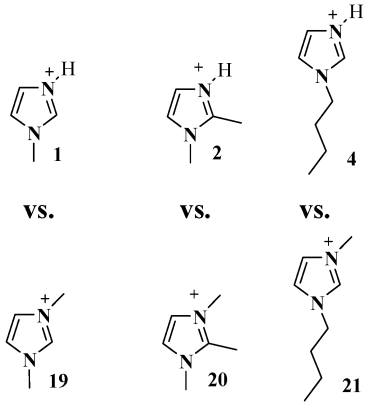

Scheme 4 Protonated *vs.* alkylated salts.

Nitrate salts were obtained from the halide salts by metathesis reactions with silver nitrate, and the picrate salts were obtained from the halide precursors by ion exchange with sodium picrate followed by solvent extraction into chloroform. In all cases, the salts were obtained in high yields. The absence of halide byproducts, from the anion exchange reactions, was confirmed with a silver nitrate test. The results confirmed removal of the halide byproducts during the product extraction step. The obtained thermal data for these salts are presented in Table 1, along with the thermal data for their protonated analogs.

Comparison of thermal data for protonated and alkylated imidazolium picrate and nitrate salts–TGA and DSC analyses

The protonated ionic liquids do not differ too much in their melting points from their methylated derivatives (Table 1) with differences ranging from 2 °C to 20 °C with one exception; [1,2-diMe-3-H-IM][Pic] (**2a**) and [1,2,3-triMeIM][Pic] (**20a**) differ in melting point by 64 °C (the protonated salt is the higher melting). This melting point difference is especially surprising since it was expected that the more symmetrical cation ($[1,2,3\text{-triMeIM}]^+$) would form the higher melting salt. Similarly, the protonated [1,2-diMe-3-H-IM][NO_3] (**2b**) also melts at a higher temperature than the alkylated analog **20b**, but in this case the melting point difference was not as large.

As can be seen from the TGA data, the thermal stabilities of the protonated imidazolium nitrate salts (Fig. 7, open symbols) are much lower than their alkylated derivatives (Fig. 7, filled symbols) ranging between *ca.* 131 and 150 °C for protonated ILs, while the alkylated analogs of the salts appear to be stable in a higher temperature range between 215 and 268 °C. Nitrate salts with quaternized cations tended to be more thermally stable than the corresponding picrate (Fig. 7 *vs.* Fig. 8, filled symbols) salts, but with protonated cations, the picrate salts (Fig. 7 *vs.* Fig. 8, open symbols) tended to be approximately 70–80 °C more stable than the nitrate salts.

The rates of decomposition are also interesting. All nitrate salts demonstrated similar behavior as they decompose rapidly and almost completely before they reach 500 °C. More variable behavior is observed in the picrate derivatives which decompose in different ways depending on either being protonated or methylated, although their decomposition temperatures do not vary significantly between both classes of salts (Fig. 8). While the protonated imidazolium picrate derivatives

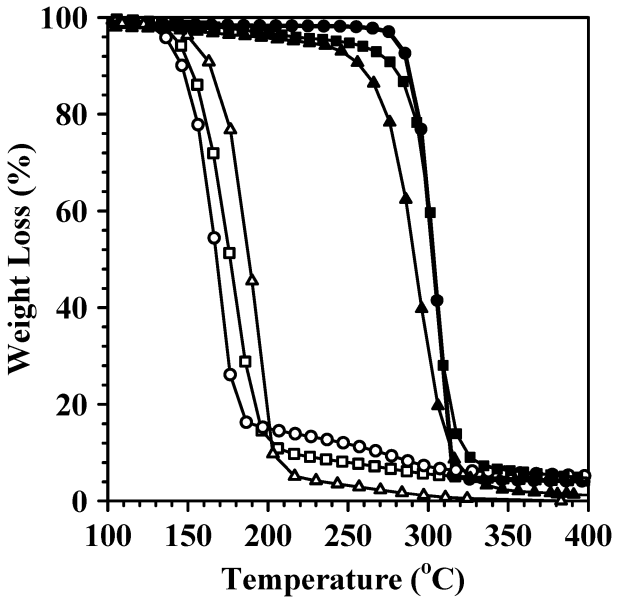

Fig. 7 Comparison of the TGA behavior between protonated (open symbols) and methylated (filled symbols) alkylimidazolium nitrate salts; protonated: (–□–) [1-Me-3-H-IM][NO_3] (**1b**), (–○–) [1,2-diMe-3-H-IM][NO_3] (**2b**), (–△–) [1-Bu-3-H-IM][NO_3] (**4b**); alkylated: (–■–) [1,3-diMeIM][NO_3] (**19b**), (–●–) [1,2,3-triMeIM][NO_3] (**20b**), (–▲–) [1-Bu-3-MeIM][NO_3] (**21b**).

(Fig. 8, open symbols) decompose in a similar way to the nitrates, which is rapid with a small quantity of solid residue left after the experiment, the alkylated imidazolium picrate derivatives (Fig. 8, filled symbols) seem to decompose at a much slower rate, with few distinguishable steps. The first step is rapid and stops after *ca.* 25–30% of the sample is decomposed, while the second

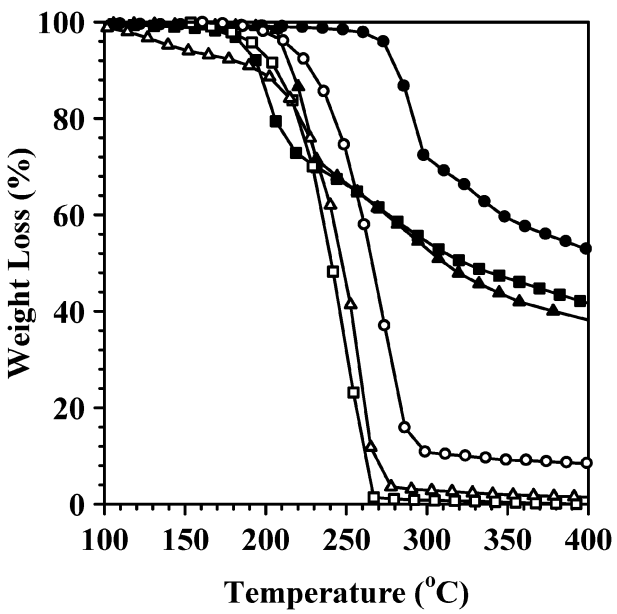

Fig. 8 Comparison of the TGA behavior between protonated (open symbols) and methylated (filled symbols) alkylimidazolium picrate salts; protonated: (–□–) [1-Me-3-H-IM][Pic] (**1a**), (–○–) [1,2-diMe-3-H-IM][Pic] (**2a**), (–△–) [1-Bu-3-H-IM][Pic] (**4a**); alkylated: (–■–) [1,3-diMeIM][Pic] (**19a**), (–●–) [1,2,3-triMeIM][Pic] (**20a**), (–▲–) [1-Bu-3-MeIM][Pic] (**21a**).

step is slower and lasts until *ca.* 40–50% of the sample is decomposed (around 300–350 °C), and the last step continues the decomposition up to 800 °C at a constant rate. These results suggest that decomposition of methylated imidazolium picrate derivatives involves different decomposition steps which occur progressively one after another and are strongly dependent on the previous step.

Accelerating rate calorimetry (ARC) analysis

Accelerating rate calorimetry (ARC) is a useful analytical technique for identification of self-heating runaway reactions and determination of information on the thermal stability of materials. Here, ARC was used to investigate the thermal decomposition of some of the synthesized salts in more detail. The decomposition temperature data for samples studied in an oxygen atmosphere in a titanium bomb are shown in Table 3. The analyzed salts show thermal stability on heating, indicated by the small residual increase in internal pressure until the thermal decomposition temperature is reached, at which point self-heating of the sample starts, resulting in an exothermic decomposition and evolution of gaseous products. The data in Table 3 describes the temperature value at which the self-heating exothermic reaction starts (T_s), the self-heating rate maximum (SHR_{max}) which describes the peak temperature change per mass unit during auto-decomposition of the sample, and pressure rate maximum (PR_{max}), which describes the peak pressure change per mass unit during auto-decomposition of the sample.

Seven ionic liquids were studied by ARC under an oxygen atmosphere: [1-Me-3-H-IM][NO_3] (**1b**), [1,2-diMe-3-H-IM][Pic] (**2a**), [1,2-diMe-3-H-MIM][NO_3] (**2b**), [1-Bu-3-H-IM][NO_3] (**4b**), 1-butylimidazolium chloride ([1-Bu-3-H-IM][Cl]) (**4c**), [1-Bu-3-MeIM][Pic] (**21a**), [1-Bu-3-MeIM][NO_3] (**21b**), and 1-butyl-3-methylimidazolium chloride ([1-Bu-3-MeIM][Cl]) (**21c**). The T_s and the SHR_{max} during their exothermic decompositions were determined and the results show that both the cation and anion components in an ionic liquid play an important role regarding its energetic properties.

From the available results for nitrate salts it was observed that alkylated imidazolium salts are much more stable than their protonated analogs. Moreover, based on the rates of the exothermic reactions among the four nitrate-based salts (Fig. 9A, B), [1-Me-3-H-IM][NO_3] (**1b**) is the most energetic, with a SHR_{max} of 1523.58 °C g^{-1} min^{-1}, then [1-Bu-3-H-IM][NO_3] (**4b**) ≫ [1-Bu-3-MeIM][NO_3] (**21b**) > [1,2-diMe-3-H-IM][NO_3] (**2b**), ordered from most to least energetic in terms of SHR_{max}.

Comparing the ARC results for [1,2-diMe-3-H-IM][NO_3] (**2b**) and [1,2-diMe-3-H-IM][Pic] (**2a**) (Table 3), it is interesting to note that the exotherm observed for [1,2-diMe-3-H-IM][Pic] (**2a**) starts at a much higher temperature but progresses much more rapidly, as shown by the SHR_{max} of 2650.48 °C g^{-1} min^{-1}, making this salt the most energetic among the analyzed compounds. Also, the pressure curves show that [1,2-diMe-3-H-IM][Pic] (**2a**) is explosive when reaching its self-decomposition temperature, at which point the pressure rate maximum (PR_{max}) reaches 2514.28 psi g^{-1} min^{-1}.

Among the series of protonated and methylated 1-butylimidazolium salts (Fig. 10 and 11), [1-Bu-3-MeIM][Pic] (**21a**) proved to be the most energetic with SHR_{max} of 1502.27 °C g^{-1} min^{-1}. In comparison, both [1-Bu-3-MeIM][NO_3] (**21b**) and [1-Bu-3-MeIM][Cl] (**21c**) were found to be much less energetic with SHR_{max} reaching only 1.31 and 1.39 °C g^{-1} min^{-1}, respectively. However, the energetic character of the protonated 1-butylimidazolium nitrate salt (**4b**) is much higher than that of the alkylated analog (**21b**), reaching a SHR_{max} value of 487.80 °C g^{-1} min^{-1}.

X-ray crystallographic studies

Single crystals were obtained for 6 salts including [1-Me-3-H-IM][Pic] (**1a**), [1,2-diMe-3-H-IM][Pic] (**2a**), [1-Me-3-H-IM][NO_3] (**1b**), [1,2-diMe-3-H-IM][NO_3] (**2b**), [1,3-diMe-IM][Pic] (**19a**), [1,2,3-triMe-IM][Pic] (**20a**), as well as two co-crystals, 1-Me-2,4-diNO_2-IM·HPic (**16a**), and 1-Me-4,5-diCN-IM·1.5 HPic (co-crystal) (**18a**) by vapor diffusion of diethyl ether into methanol at 25 °C. Data was collected on a Bruker SMART diffractometer

Table 3 Accelerating Rate Calorimetry (ARC) results for the selected protonated and alkylated imidazolium-based salts

Compound No	Ionic Liquid	T_s (°C)	SHR_{max} (Δ°C g^{-1} min^{-1})	PR_{max} (Δpsi g^{-1} min^{-1})
1b	[1-Me-3-H-IM][NO_3]	150–160	1523.58 at 254 °C	1289.74 at 264 °C
2a	[1,2-diMe-3-H-IM][Pic]	205–215	2650.48 at 271 °C	2514.28 at 262 °C
2b	[1,2-diMe-3-H-IM][NO_3]	130–140	0.69 at 173 °C 0.53 at 272 °C	0.86 at 174 °C 2.22 at 278 °C
4b	[1-Bu-3-H-IM][NO_3]	145–155	487.80 at 225 °C	1566.82 at 215 °C
4c	[1-Bu-3-H-IM][Cl]	215–225	0.90 at 269 °C	0.85 at 268 °C
21a	[1-Bu-3-MeIM][Pic]	195–205	1502.27 at 278 °C	1253.18 at 266 °C
21b	[1-Bu-3-MeIM][NO_3]	190–200	1.31 at 262 °C 0.54 at 280 °C	3.05 at 265 °C 4.74 at 283 °C
21c	[1-Bu-3-MeIM][Cl]	190–200	1.39 at 257 °C 4.05 at 381 °C	2.00 at 258 °C 1.00 at 320 °C

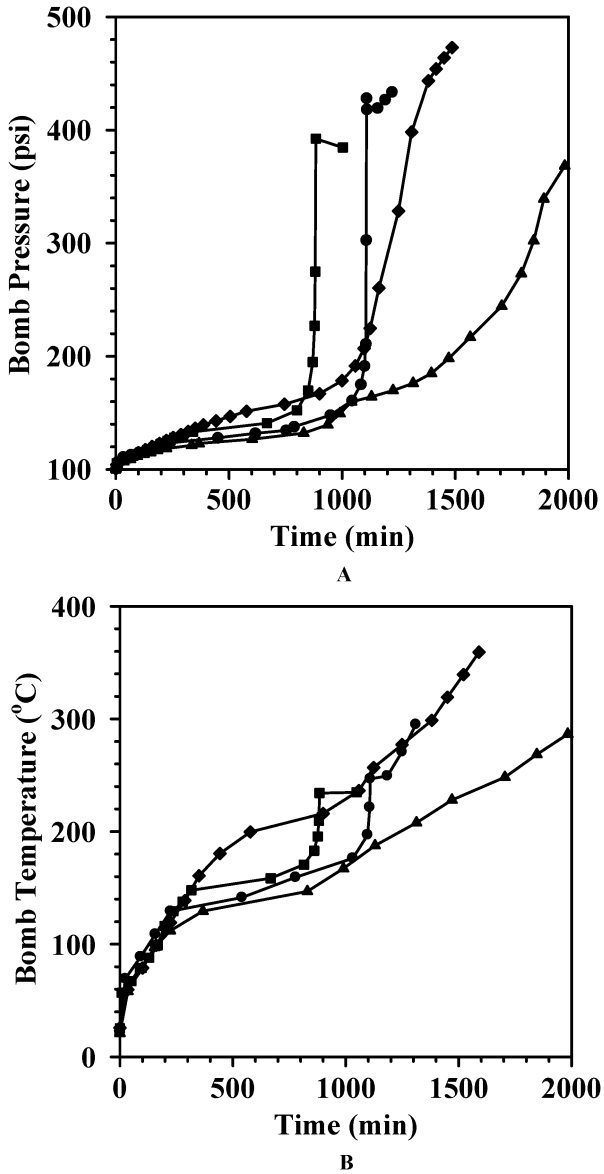

Fig. 9 ARC data for nitrate salts (A) bomb pressure *vs.* time and (B) bomb temperature *vs.* time: (–●–) [1-Me-3-H-IM][NO_3] (**1b**), (–▲–) [1,2-Me-3-H-IM][NO_3] (**2b**), (–■–) [1-Bu-3-H-IM][NO_3] (**4b**), (–◆–) [1-Bu-3-MeIM][NO_3] (**21b**).

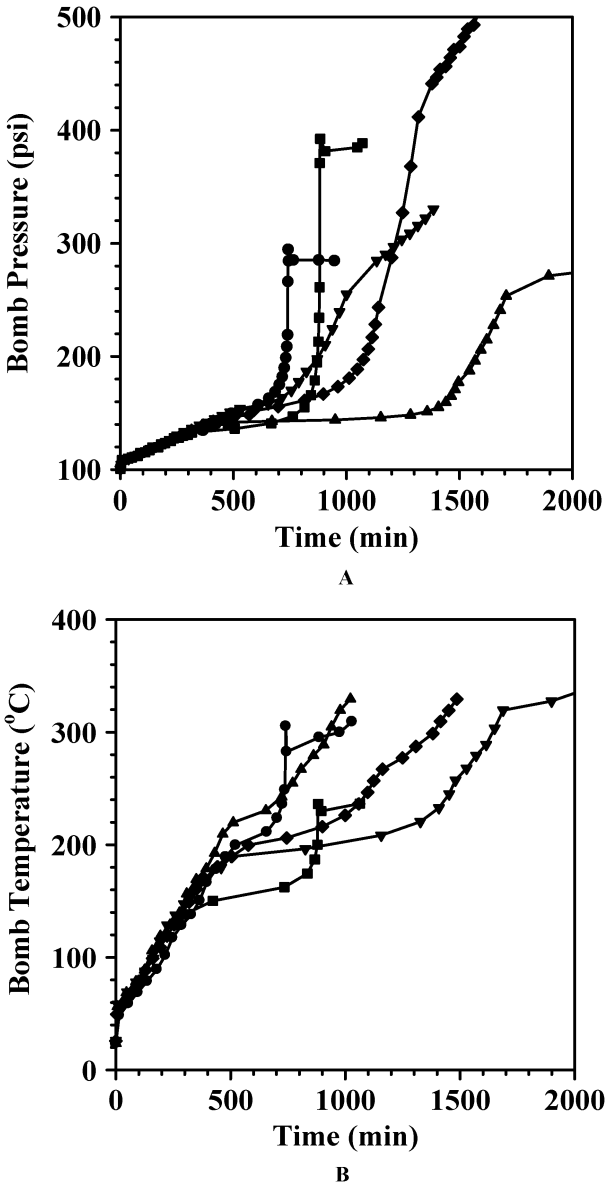

Fig. 10 ARC data for protonated and methylated 1-butylimidazolium salts (A) bomb pressure *vs.* time and (B) bomb temperature *vs.* time: (–■–) [1-Bu-3-H-IM][NO_3] (**1b**), (–▲–) [1-Bu-3-H-IM][Cl] (**1c**), (–●–) [1-Bu-3-MeIM][Pic] (**21a**), (–◆–) [1-Bu-3-MeIM][NO_3] (**21b**), (–▼–) [1-Bu-3-MeIM][Cl] (**21c**).

with a CCD area detector using graphite monochromated Mo-Kα radiation. The crystals were cooled to −100 °C during collection. Data integration, scaling, and absorption corrections were performed using the SAINT package distributed by Bruker AXS.[48] Structure solution and refinement was carried out using the SHELX-97 software suite.[49] Structures were solved using direct methods and refined by full-matrix least squares refinement against F^2. Full-occupancy non-hydrogen atoms were readily locatated from the difference map and refined anisotropically. For the 4 protic salts (**1a**, **1b**, **2a**, and **2b**), the hydrogen atoms bonded to the imidazolium nitrogen atoms were located from the difference map and the N–H bond lengths were in the range of 0.82–0.93 Å. In the co-crystal **16a**, the hydrogen atom was located from the difference map with an O–H bond length of 0.98(3) Å. In the co-crystal **18a**, there are two unique picric acid molecules; one of which lies on a crystallographic 2-fold rotation axis. The hydrogen atom on the full occupancy picric acid molecule was found from the difference map and the O–H bond length is 1.081 Å. However, the hydrogen atom on the other picric acid molecule is disordered by the crystallographic rotation axis and could not be located from the difference map; instead it was refined with 50 : 50 disorder over 2 calculated positions using a riding rotating model. **20a** showed disorder of the oxygen atoms on one of the nitro groups and the methyl groups at the 1 and 3 positions on the imidazolium ring. The disordered oxygen atoms were located from the difference map and refined anisotropically at 50 : 50 occupancy, while the methyl group hydrogen atoms were placed in calculated positions offset by 60 degrees at 50 : 50 occupancy and refined using a riding rotating model. All other

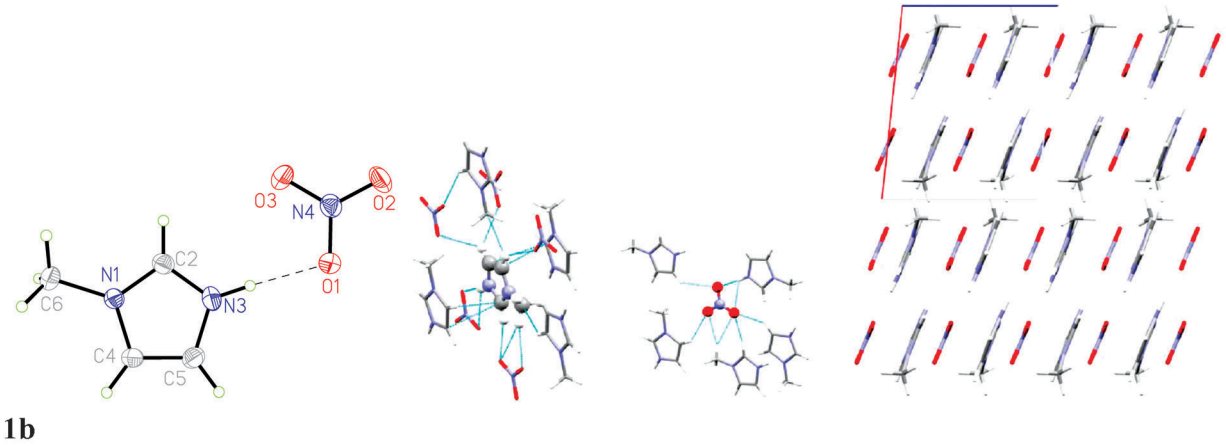

1b

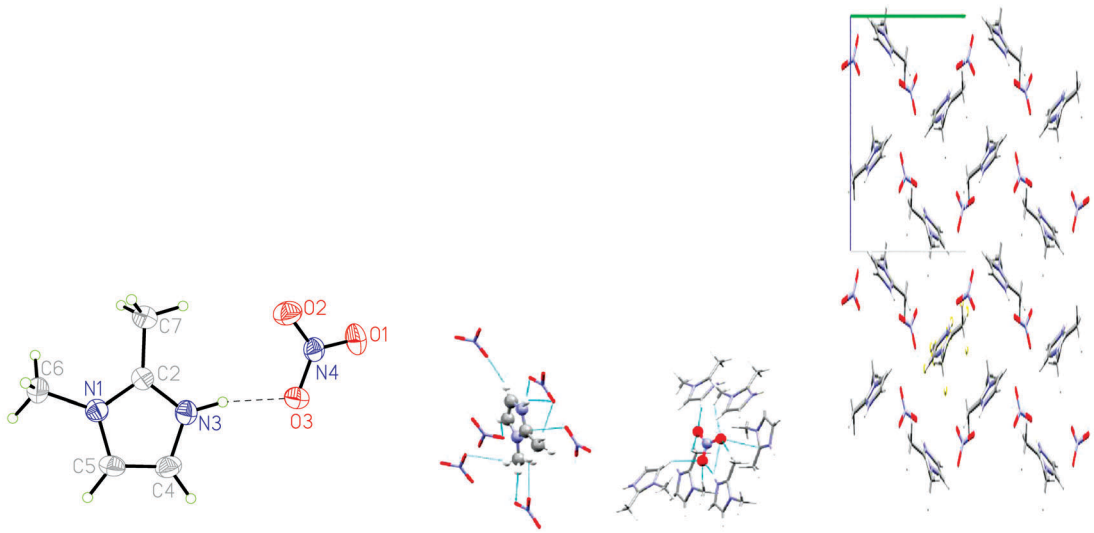

2b

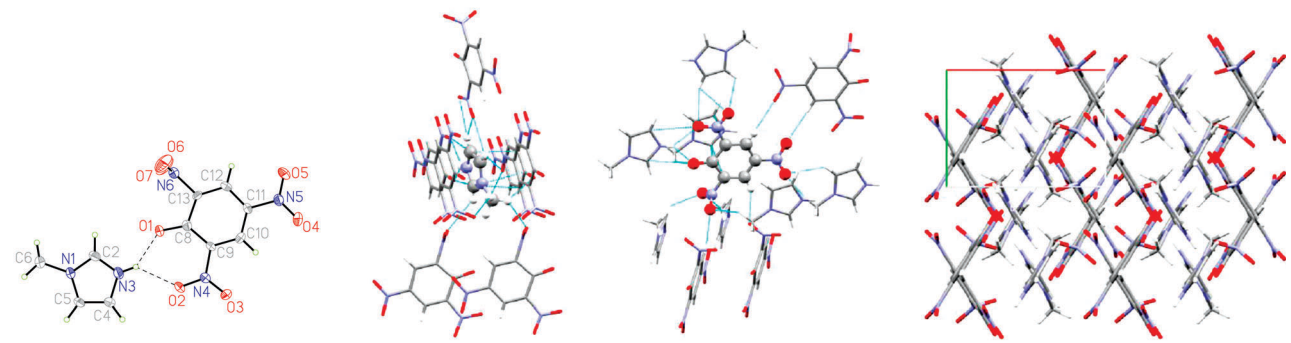

1a

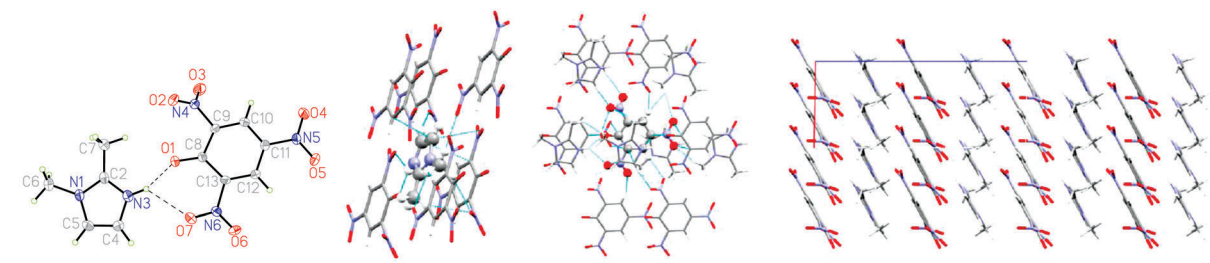

2a

Fig. 11A

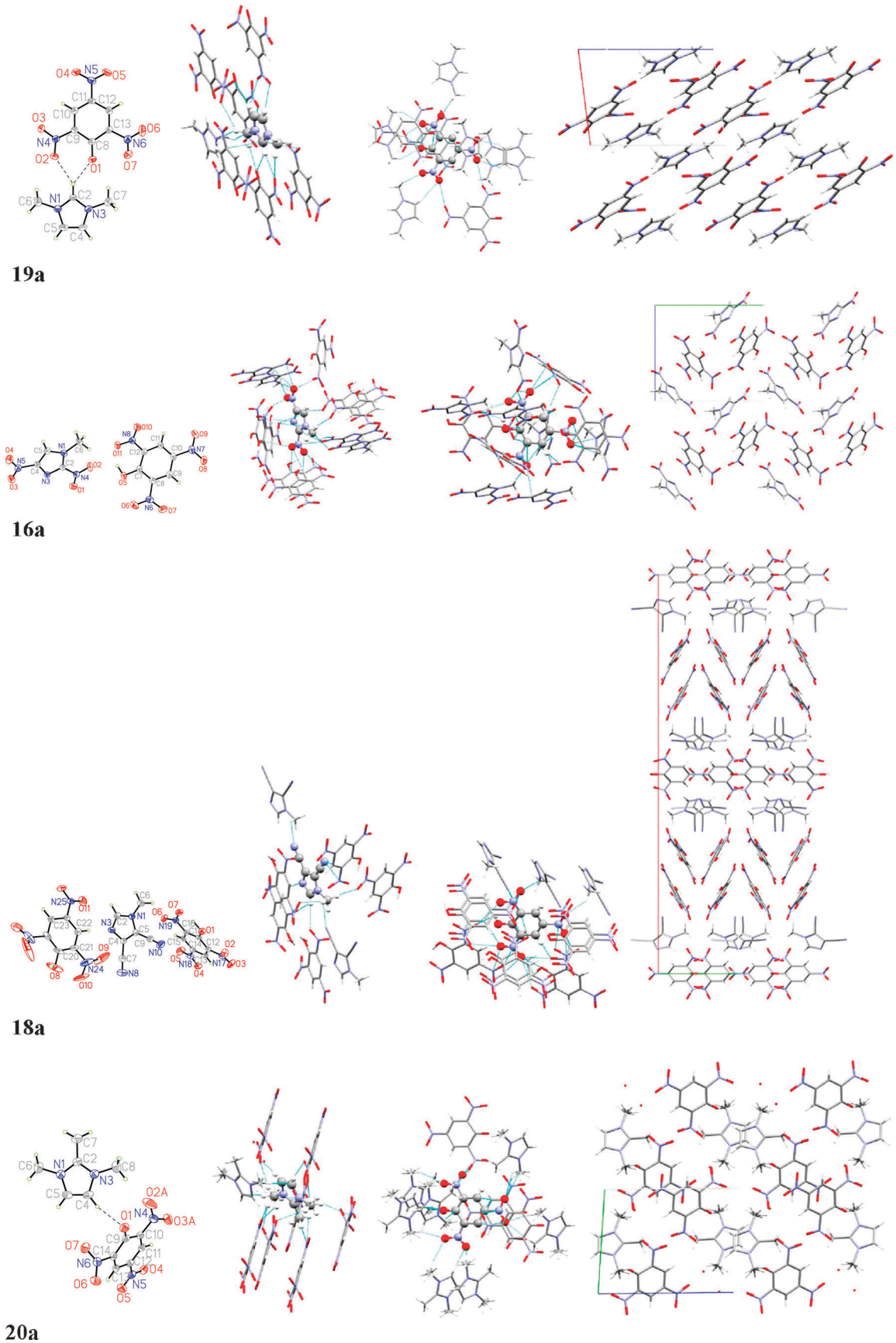

Fig. 11B From left to right: 50% probability ellipsoid diagrams of formula unit, environment around cation/imidazole, environment around anion/picric acid, and packing (axes: red = *a*, green = *b*, blue = *c*).

hydrogen atoms were placed in calculated positions and allowed to ride on their carrier atoms.

Changes in the bonds of non-hydrogen atoms were also observed which give indications of ionicity. For each of the 4 protic salts, the carbon-N1 bonds are close or statistically identical to the carbon-N3 bonds, differing by at most 0.017 Å. This is due to the delocalization of the positive charge across both sides of the ring and is observed in the dialkylimidazolium salts **19a** and **20a**. By contrast, the co-crystals show distinctly different bond lengths for the pyrrole-like and pyridine-like nitrogen atoms (N1 and N3, respectively). In **16a** the C2–N1 and C2–N3 bond lengths differ by 0.055 Å, and in **18a** they differ by 0.034 Å. The picrate anions in the 4 picrate salts (**1a**, **2a**, **19a**, and **20a**) are also structurally different from those in the co-crystals. The C–O bonds in all salts are significantly shorter than in the co-crystals while the carbon–carbon bonds to the *ortho* carbon atoms are lengthened, suggesting a greater degree of enolate character in the anion. For the nitrate salts **1b** and **2b**, the N–O bond lengths range from 1.238(2) to 1.265(2) Å, an appropriate range for nitrate anion bonds.

The bond lengths and angles for the imidazolium, imidazole, picrate, picric acid, and nitrate molecules appear to be within typical ranges. The nitrate ions in both nitrate salts are asymmetric, with two short bonds and one long one. The aromatic rings and nitrate ions are all planar. For picric acid and picrate molecules, the *para* nitro group is always coplanar with the ring while one or both of the *ortho* nitro groups are twisted out of plane or even disordered, as was modeled in **20a**.

Each of the 6 salts shows a unique combination of cation and anion interactions. This is to be expected as the protons on C2 and N3 are both hydrogen bond donors, and each cation has a different combination of protons on these sites. For the nitrate salt **1b**, the cation is surrounded by 4 cations and 5 anions. The anions all make short contacts through the hydrogen atoms on the ring: N3-H makes a directional hydrogen bond to an oxygen atom on the anion, C4-H makes a bifurcated hydrogen bond to oxygen atoms on two separate anions, and C2-H and C5-H make non-directional contacts to oxygen atoms. Two of the cation-cation contacts are between a methyl group and a ring hydrogen atom and appear to be due to the linking of two cations by short contacts to the same anion. The other cation–cation short contacts are due to stacking interactions to cations above and below the ring, which all stack C5-over-center (closest approach: C2···C4 3.329(3) Å; angle between ring planes = 4.10°). The anion is surrounded by 5 cations and no anions, and participates only in the aforementioned cation-anion contacts.

In the other nitrate salt, **2b**, the cation is surrounded by 6 anions. N3-H and C4-H make directional hydrogen bonds to nitrate ions, and C5-H and the methyl groups make non-directional contacts to nitrate ions. There is also a nitro group above the imidazolium ring plane which makes a short contact to C2. There is no stacking of cations and nearby cation rings do not overlap. The anion is surrounded by six cations and interacts *via* the aforementioned contacts. The nitro group makes short (less than the sum of the van der Waals radii) contacts to two imidazolium ions solely through contacts to the methyl groups and to a third only *via* the electrostatic interaction with C2 as opposed to **1b**, where all contacts involved acidic ring hydrogen atoms.

The picrate salts all show a combination of hydrogen bonding, dipole–dipole interactions, and stacking. In **1a**, the cation is surrounded by 7 anions. Three anions are oriented nearly coplanar with the imidazolium ring and make hydrogen bonds with the ring hydrogen atoms. N3-H makes a bifurcated hydrogen bond to the deprotonated oxygen atom and a neighboring nitro group oxygen atom on one anion, C4-H makes two non-directional contacts to nitro group oxygen atoms on another anion, and C5-H makes non-directional contacts to nitro group oxygen atoms on two separate anions. C2-H and the methyl group also make short contacts to nitro groups on anions that are not in the plane of the ring; these contacts are longer than the in-plane hydrogen bonds. The cation also stacks with two picrate anions. For one, the picrate ring stacks edge-over-center with the cation (closest approach: C2···C13, 3.381(5) Å; angle between planes = 0.89°). The *para* nitro group on another picrate also overlaps with the cation (closest approach: C5···N5, 3.503(5) Å; angle between rings = 0.55°). There are no apparent cation–cation contacts. The anion makes contacts to 7 cations and 3 anions. The anion-anion contacts are all between hydrogen atoms on C10 and C13 and nitro groups.

The cation in **2a** is surrounded by 6 anions and no cations. N3-H makes a bifurcated hydrogen bond to the deprotonated oxygen atom and a nitro group oxygen atom on a neighboring anion. There are no other directional hydrogen bonds involving the cation. The hydrogen atom on C4 makes a non-directional contact to a nitro group oxygen atom. Both methyl groups make contacts with anions, one of which (C6-H6B···O5) is rather short and directional. Anions also stack above and below the ring; one is positioned vertex-over-vertex (closest approach: C12···C5, 3.397(3) Å; angle between planes = 0.40°) and the other is positioned edge-over-center (closest approach: C14···C13, 3.277(3) Å; angle between planes = 6.71°). The anion is surrounded by 6 cations and 6 anions. Both hydrogen atoms on the picrate make short contacts to nitro groups on other anions, and the *ortho* nitro groups make short contacts to the hydrogen atoms on other anions. The *para* nitro group stacks over the C–O bond of another anion forming a dipole–dipole contact between the nitro nitrogen atom and O at 3.015(2) Å.

The cation in **19a** is surrounded by 6 anions and no cations. C2-H makes a bifurcated hydrogen bond to the deprotonated oxygen atom and a neighboring nitro group oxygen atom, C4-H forms a directional hydrogen bond to a nitro group oxygen atom. The C4 and C5 hydrogen atoms also interact with the nitro group on another cation to form a 7-membered ring. One of the methyl groups also makes short contacts to nitro groups on 3 separate anions. Two anions make contacts from above and below the imidazolium ring plane. One is a dipole–dipole interaction between the *para* nitro group and C2, and the other is through vertex-over-vertex stacking of the picrate and imidazolium rings (closest approach: C2···C11, 3.344(3) Å; angle between planes = 2.82°). The anion is surrounded by 6 cations and 3 anions. One of the anion-anion contacts appears to be due to sharing of a hydrogen atom on the cation rather than an anion-anion interaction. The anion stacks edge over center with one anion (closest approach: C8–10, 3.210(3) Å, angle between planes = 0°) and dimerizes with another anion through contacts between O1 and C8.

20a has the weakest hydrogen bond donors of the cations and, incidentally, the most disorder, with the methyl groups on N1 and N3 being disordered over 2 positions and one of the *ortho* nitro groups also being disordered over 2 positions. The cation is surrounded by 7 anions and 1 cation. The hydrogen atoms on C4 makes a directional hydrogen bond to the deprotonated oxygen atom, and the hydrogen atom on C5 makes a directional hydrogen bond to a nitro group oxygen atom. The methyl groups are involved in weaker short contacts to nitro groups. There is also vertex-over-vertex (closest approach: C4···C4, 3.188(3) Å; angle between planes = 0°) and edge-over-center (closest approach: C4···N1, 3.460(3) Å; angle between planes = 0°) stacking between cations. The anion is surrounded by 7 cations and 3 anions. One of the anions is stacked edge-over-edge (closest approach: C11···C12, 3.318(2) Å, angle between planes = 0°) which positions the *para* nitro group over C–O and N–O dipoles of the other anion. The other two anions interact through dipole–dipole interactions between antiparallel N–O bonds.

Interestingly, the co-crystal **16a** only has one strong hydrogen bonding group in the picric acid molecule which is involved in an internal hydrogen bond, so hydrogen bonding between molecules is not prevalent. Instead, interactions between the electron withdrawn carbon and nitro group nitrogen atoms with electron-rich oxygen and imidazole-nitrogen atoms are the main source of short contacts. The 2,4-dinitro-3-methylimidazole molecule is surrounded by 3 imidazole molecules and 7 picric acid molecules. The ring nitrogen atom N3 makes short contacts to carbon atoms on a picric acid molecule. The carbon atoms C4 and C5 make short contacts to nitro groups on two different picric acid molecules. The oxygen atom on the C2 nitro group makes short contacts to carbon atoms on two separate picric acid rings, and an oxygen atom on the C4 nitro group makes short contacts to the nitro group nitrogen atoms on neighboring picric acid and imidazole molecules. The other nitro group oxygen atoms are the only atoms on the imidazole which interact with hydrogen atoms; one of which interacts with the –OH group on a picric acid molecule, and, while the other interacts with a picric acid ring hydrogen atom. The methyl group makes short contacts to nitro groups on a picric acid molecule and 2 imidazole molecules *via* the hydrogen atoms. The ring hydrogen atom on C4 does not make any short contacts, as it does not have the acidity seen on an imidazolium cation. The picric acid molecules in **16a** are surrounded by 7 imidazole molecules and 4 picric acid molecules. In addition to the imidazole-picric acid contacts discussed, the picric acid molecules interact with each other through two kinds of contacts. One of the *ortho* nitro groups makes short contacts to ring hydrogen atoms in one direction, and in a perpendicular direction the –OH group and the *para* nitro group stack over each other through dipole–dipole interactions.

In **18a**, the 1-methyl-4,5-dicyanoimidazole molecule is surrounded by 2 imidazole molecules and 6 picric acid molecules. The contacts between imidazole molecules occur between nitrile groups and methyl groups at the extremity of the molecule and are not very short. The C2 hydrogen atom makes non-directional hydrogen bonds to nitro groups on two picric acid molecules. N3 accepts a directional hydrogen bond from the hydrogen atom on the picric acid ring, and the nitrile carbon atom C7 makes a short contact to a picric acid nitro oxygen atom. The nitrile nitrogen atom N10 makes a short contact to a nitro group nitrogen atom, and the methyl group makes short contacts to nitro group oxygen atoms in addition to the nitrile group of the other imidazole. The picric acid molecule which occupies a special position is surrounded by 6 imidazole molecules and 4 picric acid molecules. The –OH group makes a hydrogen bond to the nitro group of a symmetry-equivalent picric acid molecule next to it and receives the same hydrogen bond at its *para* nitro group. Nitro groups on picric acid molecules above and below the ring also make short contacts to carbon atoms on the ring. The other picric acid molecule is surrounded by 3 imidazole molecules and 6 picric acid molecules, all of which are its symmetry equivalents. Two of the picric acid molecules form N–O dipole–dipole interactions. Two interact with the hydrogen atom on the ring –OH group which engages in an internal hydrogen bond. One makes short contacts between a ring carbon atom and a nitro oxygen atom, as well as the ring hydrogen atom and a nitro oxygen atom. The last one appears to be linked through interactions to an imidazole ring and forms a contact which does not appear to due to an interaction.

The packing in **1b** consists of alternating layers of cations and anions stacking along the *c* axis. The layers are organized along the *ab* plane. Anion-cation hydrogen bonding propagates in 2-dimensional sheets roughly along the *ab* diagonal, and cation–cation pi–pi stacking propagates in chains down the *c* axis. The other nitrate salt, **2b**, has a similar salt-like packing with the notable exception that there is no cation–cation stacking. Alternating layers of cations and anions form perpendicular to the *c* axis. The cation–anion hydrogen bonding propagates in zigzag chains along roughly along *b*.

In **1a** hydrogen bonding organizes the cations and anions into infinite 1-d chains which are hydrogen bonded to each other to form pairs of antiparallel chains. The pairs of chains stack perpendicular to the hydrogen bonding direction *via* cation–anion stacking interactions to form infinite 2-d sheets, each 2 molecules wide. These sheets run roughly along the *ac* diagonals and alternating (non-hydrogen bonded) sheets are rotated 180° from each other about the *a* axis.

In **2a** the anions are organized into sheets perpendicular to *c* by anion-anion hydrogen bonding along *b* and anion-anion stacking along *a*. The cations are organized into sheets through their interactions with the anions. This results in a salt-like packing consisting of alternating sheets of cations and anions going along the *c* axis.

In **19a** chains of alternating cations and anions form along the *ac* diagonal plane. Each chain stacks with an antiparallel chain through cation-cation and anion-anion stacking, and these chain pairs go on to stack through cation–anion stacking to form sheets. There are no strong interactions between these sheets.

In **20a** the packing is salt-like, with the cations and anions arranged in columns along c through cation–cation or anion–anion stacking. The columns are surrounded by columns of counter ions forming a 3-d lattice.

The packing in **16a** resembles an inclusion compound. The picric acid molecules are self-organized into pleated sheets perpendicular to *c*. These sheets are bridged to each other on both sides by imidazole molecules. The imidazole molecules are also arranged in pleated sheets but there are no interactions which suggest this is self-organized.

The packing in **18a** is interesting and may represent a case of arrested crystallization. The two unique picric acid molecules never interact with each other and as a result there are 3 distinct zones in the packing: One of the picric acid molecules is self-organized into sheets composed of zigzag chains, and the other is organized into a sheet of stacked, head-to-tail hydrogen bonded molecules. The imidazole molecules bridge these two sheets together.

Of the 6 salts which formed crystals, the picrate salts typically had more short contacts, especially anion–anion contacts, than nitrate salts which is in agreement with the higher melting points recorded. The melting point data also shows a relationship between hydrogen bond donor availability and melting point. The protic picrate salts both have higher melting points than their aprotic analogs, The lowest melting of all the picrate salts, **16a**, has only the least acidic C4 and C5 protons available for hydrogen bonding.

Crystallographic data. **1a**–$C_{10}H_9N_5O_7$; M = 311.12; Monoclinic, space group = $P2_1/c$; a = 8.018(2) Å, b = 5.885(2) Å, c = 27.215(7) Å; β = 94.798(5)°; V = 1279.7(6) Å^3; Z = 4; T = 173 K; λ(Mo-Kα) = 0.71073 Å; $R_1 > 2\sigma$ = 0.0580, wR^2 for all reflections = 0.1216. **1b**–$C_4H_7N_3O_3$; M = 145.13; Monoclinic, space group $P2_1/c$; a = 8.957(7) Å, b = 9.917(7) Å, c = 7.143(6) Å; β = 96.05(1)°; V = 630.9(8) Å^3; Z = 4; T = 173 K; λ(Mo-Kα) = 0.71073 Å; $R_1 > 2\sigma$ = 0.0347, wR^2 for all reflections = 0.0929. **2a**–$C_{11}H_{11}N_5O_7$; M = 325.25; Monoclinic, space group = Cc; a = 6.076(2) Å, b = 15.089(5) Å, c = 14.771(4) Å; β = 90.949(5)°; V = 1354.0(7) Å^3; Z = 4; T = 173 K; λ(Mo-Kα) = 0.71073 Å; Flack parameter = 0.7(8); $R_1 > 2\sigma$ 0.0228, wR^2 for all reflections = 0.0593. **2b**–$C_5H_9N_3O_3$; M = 159.15; Monoclinic, space group = $P2_1/n$; a = 7.863(1) Å, b = 13.001(2) Å, c = 7.971(1) Å; β = 111.871(3)°; V = 756.2(2) Å^3; Z = 4; T = 173 K; λ(Mo-Kα) = 0.71073 Å; $R_1 > 2\sigma$ = 0.0343, wR^2 for all reflections = 0.0918. **16a**–$C_{10}H_7N_7O_{11}$; M = 401.23; Monoclinic, space group = $P2_1$; a = 6.287(1) Å, b = 11.646(2) Å, c = 10.307(2) Å; β = 93.367(3)°; V = 753.3(2) Å^3; Z = 2; T = 173 K; λ(Mo-Kα) = 0.71073 Å; Flack parameter = −0.4(8); $R_1 > 2\sigma$ = 0.0236; wR^2 = 0.0558. **18a**–$C_{15}H_{8.5}N_{8.5}O_{10.5}$; M = 475.80; Orthorhombic, space group = Pbcn; a = 43.98(1) Å; b = 8.850(2) Å; c = 9.627(2) Å; $\alpha = \beta = \gamma$ = 90°; V = 3747(2) Å^3; Z = 8; T = 173 K; λ(Mo-Kα) = 0.71073 Å; $R_1 > 2\sigma$ 0.0678; wR^2 for all reflections = 0.1367. **19a**–$C_{11}H_{11}N_5O_7$; M = 325.25; Triclinic, space group = $P\bar{1}$; a = 7.210(2) Å; b = 9.615(2) Å; c = 10.265(2) Å; α = 78.308(3)°; β = 82.099(4)°, γ = 85.773(4)°; V = 689.5(3) Å^3; Z = 2; T = 173 K; λ(Mo-Kα) = 0.71073 Å; $R_1 > 2\sigma$ = 0.0592, wR^2 = 0.1305. **20a**–$C_{12}H_{13}N_5O_7$; M = 339.27; Triclinic, space group = $P\bar{1}$; a = 7.250(2) Å, b = 9.107(3) Å, 11.946(4) Å; α = 83.270(5)°, β = 74.608(5)°, γ = 79.684(5)°; V = 746.1(4) Å^3; Z = 2; T = 173 K; λ(Mo-Kα) = 0.71073 Å; $R_1 > 2\sigma$ = 0.0352, wR^2 for all reflections = 0.0913.

Experimental

Chemicals

1-Methylimidazole (1-MeIM, **1**) (98%), 1,2-dimethylimidazole (1,2-diMeIM, **2**) (98%), and 1-butylimidazole (1-BuIM, **4**) (98%) were purchased from Aldrich. 1-Methyl-2-nitroimidazole (1-Me-2-NO_2-IM, **8**), 1,2-dimethyl-5-nitroimidazole (1,2-diMe-5-NO_2-IM, **9**), 1-ethyl-2-nitroimidazole (1-Et-2-NO_2-IM, **10**), 1-ethyl-4-nitroimidazole (1-Et-4-NO_2-IM, **11**), 1-methyl-2,4-dinitroimidazole (1-Me-2,4-diNO_2-IM, **16**), 1-methyl-4,5-dinitroimidazole (1-Me-4,5-diNO_2-IM, **17**), and 1-methyl-4,5-dicyanoimidazole (1-Me-4,5-diCN-IM, **18**) were prepared following our recently published procedure.[41] All imidazoles were distilled prior to use. Nitric acid (69.5% w/w water solution) was obtained from Fisher (Waltham, MA). Picric acid (containing not less than 30% w/w water) was obtained from MERCK (Darmstadt, Germany). Acids were used as diluted solutions, 3 M HNO_3 solution in water, and 0.1 M picric acid solution in EtOH.

NMR spectra were obtained in $CDCl_3$ (unless otherwise stated) with TMS as the internal standard for ^{1}H (300 MHz) or the solvent as the internal standard for ^{13}C (75 MHz). All of the chemicals were employed as supplied.

Thermogravimetric analyses (TGA) were performed using a TGA 2950, TA Instruments, Inc. (New Castle, DE). These experiments were conducted under air atmosphere and measured in the dynamic heating regime. Samples between 5–15 mg were heated from 30–500 °C under constant heating ramp of 5 °C min^{-1} with a 30 min isotherm at 75 °C. Temperatures reported for the decomposition profiles for all materials were established as the onset temperature for decomposition of the first 5% of the sample ($T_{5\%onset}$).

Melting point/glass transition analyses were performed by differential scanning calorimetry (DSC) using a DSC 2920 Modulated DSC, TA Instruments, Inc. (New Castle, DE) cooled with a liquid nitrogen cryostat. The calorimeter was calibrated for temperature and cell constants using indium (T_m = 156.61 °C; C = 28.71 J g^{-1}). Data were collected at atmospheric pressure, where samples were initially heated at a rate of 5 °C min^{-1} to a temperature not to exceed 50 °C below the measured $T_{5\%onset}$ (obtained from TGA). The sample was then held for a 5 min isotherm prior to two cycles of cooling and heating (back to upper temperature limit from first heating) at a rate of 5 °C min^{-1} spaced by 5 min isothermal holding at lower (T = −100 °C, unless otherwise stated) and upper (as indicated above) endpoint temperatures. Samples between 5–15 mg were used in aluminum sample pans (sealed, then perforated with a pin-hole to equilibrate pressure resulting from potential expansion of evolved gases). The DSC was adjusted so that zero heat flow was between 0 and −0.5 mW, and the baseline drift was less than 0.1 mW over the temperature range of 0–180 °C. An empty sample pan served as the reference. Temperatures reported for the glass transition (T_g) and melting (T_m) were established as the onset temperature for the endothermic change in heat flow measured through the material and as the onset temperature for the exothermic change in heat flow measured in the case of observed crystallization (T_{cryst}).

Accelerating rate calorimetric (ARC) measurements were carried out with a modified Arthur D. Little ARC 2000™, which allows samples to be run in a specific atmosphere.[50] Titanium bombs (1 inch o.d., from Tricor Metals, Inc.) were used for all the ARC runs. The standard ARC operational mode of Heat-Wait-Search (HWS) was adopted.

Procedure for alkylimidazoles (*method A*) (3, 7, 13–15)

A mixture of appropriate imidazole (10 mmol), alkyl bromide (12 mmol), potassium carbonate (3.32 g, 24 mmol), and tetrabutylammonium bromide (0.032 g, 0.1 mmol) in acetonitrile (50 mL) was stirred vigorously under reflux for 2 h. After cooling to room temperature, the precipitate was filtered off and washed with acetonitrile. The filtrate was evaporated, and the crude products were purified *via* column chromatography using ethyl acetate/hexane.

Procedure for alkylimidazoles (*method B*) (3, 5–7, 12)

The appropriate imidazole (50 mmol) was dissolved in DMF (10 mL). Potassium *tert*-butoxide (6.7 g, 60 mmol) was added at 0–5 °C followed by the addition of appropriate alkyl bromide (72 mmol). The reaction mixture was stirred at room temperature overnight. Water (20 mL) was added to the mixture. The solution was extracted with ethyl acetate (3 × 40 mL). The extract was washed with brine and dried over anhydrous magnesium sulfate. The solvent was evaporated under reduced pressure (bath 60–70 °C) to remove DMF and the residue was purified *via* column chromatography using ethyl acetate/hexane to give the desired *N*-alkylimidazoles.

1-Propylimidazole (1-PrIM, 3)[51]. Oil, 60% yield, ^{1}H NMR (300 MHz, [D_1] $CHCl_3$) δ, 0.91 (t, J = 7.4 Hz, 3H), 1.85–1.73 (m, 2H), 3.89 (t, J = 7.1 Hz, 2H), 6.90 (s, 1H), 7.04 (s, 1H), 7.45 (s, 1H), ^{13}C NMR (75 MHz, [D_1] $CHCl_3$) δ 10.8, 24.1, 48.3, 118.5, 129.0, 136.8.

1-Butyl-2-methylimidazole (1-Bu-2-MeIM, 5)[52]. Oil (87%[b]); ^{1}H NMR (300 MHz, [D_1] $CHCl_3$) δ 0.94 (t, J = 7.3 Hz, 3H), 1.33 (m, 2H), 1.72–1.67 (m, 2H), 2.36 (s, 3H), 3.81 (t, J = 7.2 Hz, 2H), 6.80 (d, J = 1.0 Hz, 1H), 6.88 (d, J = 1.0 Hz, 1H); ^{13}C NMR (75 MHz, [D_1] $CHCl_3$) δ 12.8, 13.3, 19.5, 32.5, 45.5, 118.8, 126.7, 144.0. Anal. Calcd for $C_8H_{14}N_2$: C, 69.52; H, 10.21; N, 20.27. Found: C, 68.91; H, 10.62; N, 20.02.

1-Pentyl-2-methylimidazole (1-Pent-2-MeIM, 6)[52]. Oil, 92%[b] yield, ^{1}H NMR (300 MHz, [D_1] $CHCl_3$) δ 0.90 (t, J = 7.0 Hz, 3H), 1.37–1.26 (m, 4H), 1.75–1.65 (m, 2H), 2.35 (s, 3H), 3.79 (t, J = 7.1 Hz, 2H), 6.79 (d, J = 1.2 Hz, 1H), 6.88 (d, J = 1.2 Hz, 1H), ^{13}C NMR (75 MHz, [D_1] $CHCl_3$) δ, 12.6, 13.5, 21.8, 28.2, 30.0, 45.6, 118.6, 126.5, 143.8. Anal. Calcd for $C_9H_{16}N_2$: C, 71.01; H, 10.59; N, 18.40. Found: C, 70.25; H, 11.09; N, 17.96.

1-Hexylimidazole (1-HexIM, 7)[52]. Oil, 44%[a] and 72%[b] yield, ^{1}H NMR (300 MHz, [D_1] $CHCl_3$) δ, 0.88 (t, J = 7.6 Hz, 3H) 1.33–1.26 (m, 6H), 1.75 (p, J = 14.4 Hz, J = 7.0 Hz, 2H), 3.91 (t, J = 7.1 Hz, 2H), 6.90 (t, J = 1.2 Hz, 1H), 7.04 (t, J = 1.0 Hz, 1H), 7.45 (s, 1H); ^{13}C NMR (75 MHz, [D_1] $CHCl_3$) δ 13.6, 22.1, 25.8, 30.7, 30.8, 46.6, 118.4, 128.9, 136.7. Anal. Calcd for $C_9H_{16}N_2$: C, 71.01; H, 10.59; N, 18.40. Found: C, 69.96; H, 10.98; N, 18.39.

1-Isopropyl-4-nitroimidazole (1-*i*-Pr-4-NO_2-IM, 12). Plates from ethyl acetate/hexane 78%[b] yield, mp 50–53 °C; ^{1}H NMR (300 MHz, [D_1] $CHCl_3$) δ 1.59 (d, J = 6.7 Hz, 6H), 4.56–4.47 (m, 1H), 7.58 (d, J = 1.1 Hz, 1H), 7.91 (d, J = 1.3 Hz, 1 H), ^{13}C NMR (75 MHz, [D_1] $CHCl_3$) δ 23.3, 50.9, 117.3, 134.3, 147.9. Anal. Calcd for $C_6H_9N_3O_2$: C, 46.45; H, 5.85; N, 27.08. Found: C, 46.85; H, 5.82; N, 27.11.

1-Butyl-2-methyl-4-nitroimidazole (1-Bu-2-Me-4-NO_2-IM, 13). Microcrystals from ethyl acetate/hexane, 84%[a] yield, mp 58–60 °C, ^{1}H NMR (300 MHz, [D_1] $CHCl_3$) δ 0.99 (t, J = 7.4 Hz, 3H), 1.46–1.33 (m, 2H), 1.84–1.74 (m, 2H), 2.44 (s, 3H), 3.94 (t, J = 7.3 Hz, 2H), 7.71 (s, 1H), ^{13}C NMR (75 MHz, [D_1] $CHCl_3$) δ 13.0, 13.4, 19.5, 32.1, 46.9, 119.5, 144.5, 146.2. Anal. Calcd for $C_8H_{13}N_3O_2$: C, 52.45; H, 7.15; N, 22.94. Found: C, 52.80; H, 7.33; N, 22.87.

1-Pentyl-2-methyl-4-nitroimidazole (1-Pent-2-Me-4-NO_2-IM, 14). Microcrystals from ethyl acetate/hexane, 65%[a] yield, mp 35–37 °C, ^{1}H NMR (300 MHz, [D_1] $CHCl_3$) δ 0.93 (t, J = 6.7 Hz, 3H), 1.40–1.32 (m, 4H), 1.85–1.75 (m, 2H), 2.44 (s, 3H), 3.92 (t, J = 7.4 Hz, 2H), 7.70 (s, 1H), ^{13}C NMR (75 MHz, [D_1] $CHCl_3$) δ 13.1, 13.7, 22.1, 28.4, 29.9, 47.2, 119.5, 144.5, 146.3. Anal. Calcd for $C_9H_{15}N_3O_2$: C, 54.81; H, 7.67; N, 21.30. Found: C, 55.13; H, 7.90; N, 21.22.

1-Hexyl-4-nitroimidazole (1-Hex-4-NO_2-IM, 15). Microcrystals from ethyl acetate/hexane, 62%[a] yield, mp 39–41 °C, ^{1}H NMR (300 MHz, [D_1] $CHCl_3$) δ 0.89 (t, J = 6.9 Hz, 3H), 1.36–1.28 (m, 6H), 1.90–1.80 (m, 2H), 4.04 (t, J = 7.1 Hz, 2H), 7.46 (d, J = 1.3 Hz, 1H), 7.79 (d, J = 1.4 Hz, 1H), ^{13}C NMR (75 MHz, [D_1] $CHCl_3$) δ 13.7, 22.2, 25.8, 30.5, 30.9, 48.3, 119.1, 135.9, 147.9. Anal. Calcd for $C_9H_{15}N_3O_2$: C, 54.81; H, 7.67; N, 21.30. Found: C, 55.13; H, 7.93; N, 21.10.

General procedure for preparation of protonated imidazolium nitrate and picrate salts

A variety of acid–base paired, protonated imidazolium salts were prepared using a neutralization reaction procedure.[53] The appropriate imidazole (0.6 mmol) was dissolved in EtOH (3 mL) and a solution of the appropriate acid (0.6 mmol; 3% excess of nitric acid was used for the preparation of nitrates) was added dropwise to the imidazole solution with stirring at 40 °C. All of the neutralization reactions were exothermic. The solution was stirred for up to 10 h at 40 °C, after which the solvent was removed on a rotary evaporator, under reduced pressure, at 50 °C. Reaction progress was monitored using TLC chromatographic techniques, using chloroform and methanol as eluent, comparing the signatures of the obtained products with the TLC signature of the starting materials. Solid products were washed with cold EtOH to remove any unreacted substrates. Similarly, liquid samples were washed with dry acetone. Pure products were obtained in 82–99% yields after drying under vacuum at 40 °C for 10 h. The reactions with 1-methylimidazolium, 1,2-dimethylimidazolium, and 1-butylimidazolium salts were performed using the same procedure but on larger scale (50 mmol).

1-Methylimidazolium Picrate ([1-Me-3-H-IM][Pic]) (1a). Yellow solid, 98% yield; ^{1}H NMR (360 MHz, [D_6] DMSO) δ = 3.85 (s, 3H, N-CH_3), 7.61 (s, 1H, C5-H), 7.65 (s, 1H, C4-H), 8.58 (s, 2H, picrate), 8.94 (s, 1H, N-H); ^{13}C NMR (90 MHz, [D_6] DMSO) δ = 35.24 (*N*-CH_3), 120.14, 122.97 (C4/5), 124.13 (picrate), 125.14 (picrate), 135.87 (C2), 141.83 (picrate), 160.77 (picrate).

1,2-Dimethylimidazolium Picrate ([1,2-diMe-3-H-IM][Pic]) (2a). Yellow solid, 98% yield; ^{1}H NMR (360 MHz, [D$_6$] DMSO) δ = 2.54 (s, 3H, C2-CH$_3$), 3.72 (s, 3H, N-CH$_3$), 7.51 (s, 1H, C5-H), 7.56 (s, 1H, C4-H), 8.58 (s, 2H, picrate); ^{13}C NMR (90 MHz, [D$_6$] DMSO) δ = 10.22 (C2-CH$_3$), 33.84 (*N*-CH$_3$), 117.59, 122.95 (C4/5), 124.11 (picrate), 125.15 (picrate), 141.84 (picrate), 144.41 (C2), 160.77 (picrate).

1-Propylimidazolium Picrate ([1-Pr-3-H-IM][Pic]) (3a). Yellow solid, 95% yield; ^{1}H NMR (360 MHz, [D$_6$] DMSO) δ = 0.82 (t, 3H, –CH$_3$), 1.80 (m, 2H, –CH$_2$–CH$_3$), 4.12 (t, 3H, N-CH$_2$–), 7.59 (s, 1H, C5-H), 7.70 (s, 1H, C4-H), 8.59 (s, 2H, picrate), 8.93 (s, 1H, C2-H); ^{13}C NMR (90 MHz, [D$_6$] DMSO) δ = 10.20 (–CH$_3$), 22.73 (–CH$_2$–CH$_3$), 49.44 (N–CH$_2$–), 120.79, 121.36 (C4/C5), 123.85 (picrate), 124.91 (picrate), 135.22 (C2), 141.54(picrate), 160.57 (picrate).

1-Butylimidazolium Picrate ([1-Bu-3-H-IM][Pic]) (4a). Yellow viscous liquid, 98% yield; ^{1}H NMR (360 MHz, [D$_6$] DMSO) δ = 0.90 (t, 3H, –CH$_3$), 1.23 (sextet, 2H, –CH$_2$–), 1.76 (p, 2H, –CH$_2$–), 4.13 (t, 2H, N–CH$_2$–), 7.52 (s, 1H, C5-H), 7.65 (s, 1H, C4-H), 8.60 (s, 2H, picrate), 9.19 (s, 1H, C2-H); ^{13}C NMR (90 MHz, [D$_6$] DMSO) δ = 13.34 (–CH$_3$), 18.93 (–CH$_2$–CH$_3$), 31.02 (–CH$_2$–), 46.52 (N–CH$_2$–), 118.20, 121.85 (C4/C5), 124.15 (picrate), 125.11 (picrate), 141.55 (picrate), 144.52 (C2), 160.75 (picrate).

1-Butyl-2-methylimidazolium Picrate ([1-Bu-2-Me-3-H-IM][Pic]) (5a). Yellow solid, 98% yield; ^{1}H NMR (360 MHz, [D$_6$] DMSO) δ = 0.91 (t, 3H, –CH$_3$), 1.29 (m, 2H, –CH$_2$–CH$_3$), 1.71 (p, 2H, –CH$_2$–CH$_2$–), 2.58 (s, 3H, C2–CH$_3$), 4.07 (t, 3H, N–CH$_2$–), 7.56 (s, 1H, C5-H), 7.64 (s, 1H, C4-H), 8.59 (s, 2H, picrate); ^{13}C NMR (90 MHz, [D$_6$] DMSO) δ = 10.23 (–CH$_3$), 13.38 (C2–CH$_3$), 18.96 (–CH$_2$–CH$_3$), 31.01 (–CH$_2$–), 46.52 (N–CH$_2$–), 118.11, 121.81 (C4/C5), 124.09 (picrate), 125.07 (picrate), 141.47 (picrate), 144.06 (C2), 160.83 (picrate).

1-Pentyl-2-methylimidazolium Picrate ([1-Pent-2-Me-3-H-IM][Pic]) (6a). Yellow solid, 96% yield; ^{1}H NMR (360 MHz, [D$_6$] DMSO) δ = 0.87 (t, 3H, –CH$_3$), 1.30 (m, 4H, –CH$_2$–CH$_2$–), 1.73 (p, 2H, –CH$_2$–CH$_2$–), 2.56 (s, 3H, C2–CH$_3$), 4.05 (t, 3H, N–CH$_2$–), 7.54 (s, 1H, C5-H), 7.63 (s, 1H, C4-H), 8.59 (s, 2H, picrate); ^{13}C NMR (90 MHz, [D$_6$] DMSO) δ = 10.47 (–CH$_3$), 13.92 (C2–CH$_3$), 21.77 (–CH$_2$–CH$_3$), 27.95 (–CH$_2$–), 28.88 (–CH$_2$–), 46.84 (N–CH$_2$–), 118.39, 121.92 (C4/C5), 124.39 (picrate), 125.34 (picrate), 141.37 (picrate), 144.00 (C2), 160.80 (picrate).

1-Hexylimidazolium Picrate ([1-Hex-3-H-IM][Pic]) (7a). Yellow liquid, 97% yield; ^{1}H NMR (360 MHz, [D$_6$] DMSO) δ = 0.84 (t, 3H, –CH$_3$), 1.25 (m, 6H, –CH$_2$–CH$_2$–CH$_2$–), 1.77 (p, 2H, –CH$_2$–CH$_2$–), 4.13 (t, 3H, N–CH$_2$–), 7.55 (s, 1H, C5-H), 7.68 (s, 1H, C4-H), 8.50 (s, 2H, picrate), 8.86 (s, 1H, C2-H); ^{13}C NMR (90 MHz, [D$_6$] DMSO) δ = 13.74 (–CH$_3$), 21.81 (–CH$_2$–CH$_3$), 25.17 (–CH$_2$–), 29.48 (–CH$_2$–), 30.45 (–CH$_2$–), 47.98 (N–CH$_2$–), 120.30, 121.40 (C4/C5), 124.15 (picrate), 125.10 (picrate), 135.45 (C2), 141.76 (picrate), 159.84 (picrate).

1-Methyl-2-nitroimidazolium Picrate ([1-Me-2-NO$_2$-3-H-IM][Pic]) (8a). Yellow slowly crystallizing viscous liquid; ^{1}H NMR (360 MHz, [D$_6$] DMSO) δ = 3.99 (s, 3H, N-CH$_3$), 7.15 (s, 1H, C5-H), 7.64 (s, 1H, C4-H), 8.61 (s, 2H, picrate), 11.42 (b, N–H); ^{13}C NMR (90 MHz, [D$_6$] DMSO) δ = 37.05 (N–CH$_3$), 124.46 (picrate), 125.17 (picrate), 127.47, 128.48 (C4/5), 141.76 (picrate), 151.58 (C2), 160.52 (picrate).

1,2-Dimethyl-5-nitroimidazolium Picrate ([1,2-diMe-5-NO$_2$-3-H-IM][Pic]) (9a). Yellow thin crystals, 92% yield; ^{1}H NMR (360 MHz, [D$_6$] DMSO) δ = 2.49 (s, 3H, C2-CH$_3$), 3.85 (s, 3H, N-CH$_3$), 8.27 (s, 1H, C4-H), 8.59 (s, 2H, picrate); ^{13}C NMR (90 MHz, [D$_6$] DMSO) δ = 13.05(C2-CH$_3$), 33.50 (N–CH$_3$), 124.52 (picrate), 125.13 (picrate), 129.06 (C4), 141.76 (picrate), 143.62 (C2), 150.09 (C5), 160.85 (picrate).

1-Ethyl-2-nitroimidazolium Picrate ([1-Et-2-NO$_2$-3-H-IM][Pic]) (10a). Yellow viscous liquid, 86% yield; ^{1}H NMR (360 MHz, [D$_6$] DMSO) δ = 1.38 (t, 3H, –CH$_3$), 4.40 (q, 2H, N–CH$_2$–), 7.17 (d, 1H, C5-H), 7.70 (d, 1H, C4-H), 8.59 (s, 2H, picrate), *ca.* 9.2 (b, N–H); ^{13}C NMR (90 MHz, [D$_6$] DMSO) δ = 15.56 (–CH$_3$), 44.72 (N–CH$_2$–), 124.81 (picrate), 125.14 (picrate), 127.06, 128.86 (C4/5), 141.76 (picrate), 150.22 (C2), 160.41 (picrate).

1-Ethyl-4-nitroimidazolium Picrate ([1-Et-4-NO$_2$-3-H-IM][Pic]) (11a). Yellow viscous liquid, 83% yield; ^{1}H NMR (360 MHz, [D$_6$] DMSO) δ = 1.41 (t, 3H, –CH$_3$), 4.12 (q, 2H, N–CH$_3$), 7.91 (s, 1H, C5-H), 8.48 (s, 1H, C2-H), 8.61 (s, 2H, picrate), 9.35 (b, N–H); ^{13}C NMR (90 MHz, [D$_6$] DMSO) δ = 15.70 (CH$_2$–CH$_3$), 42.51 (N–CH$_2$), 121.20 (C5), 124.31 (picrate), 125.15 (picrate), 136.95 (C2), 141.78 (picrate), 146.89 (C4), 160.58 (picrate).

1-Isopropyl-4-nitroimidazolium Picrate ([1-*i*-Pr-4-NO$_2$-3-H-IM][Pic]) (12a). Yellow solid, 91% yield; ^{1}H NMR (360 MHz, [D$_6$] DMSO) δ = 1.44 (d, 6H, –CH$_3$), 4.53 (m, 1H, N–CH–), 7.95 (s, 1H, C5-H), 8.52 (s, 1H, C2-H), 8.59 (s, 2H, picrate); ^{13}C NMR (90 MHz, [D$_6$] DMSO) δ = 22.91 (–CH$_3$), 50.59 (N–CH–), 119.84 (C5), 124.52 (picrate), 125.27 (picrate), 135.95 (C4), 141.92 (picrate), 147.14 (C2), 160.69 (picrate).

1-Butyl-2-methyl-4-nitroimidazolium Picrate ([1-Bu-2-Me-4-NO$_2$-3-H-IM][Pic]) (13a). Yellow solid, 94% yield; ^{1}H NMR (360 MHz, [D$_6$] DMSO) δ = 0.89 (t, 3H, –CH$_3$), 1.26 (m, 2H, –CH$_2$–CH$_3$), 1.69 (p, 2H, –CH$_2$–), 2.35 (s, 3H, C2-CH$_3$), 3.97 (t, 2H, N–CH$_2$–), 8.32 (s, 1H, C5-H), 8.59 (s, 2H, picrate); ^{13}C NMR (90 MHz, [D$_6$] DMSO) δ = 12.48 (–CH$_3$), 13.32 (C2–CH$_3$), 18.99 (–CH$_2$–CH$_3$), 31.44 (–CH$_2$–), 46.10 (N–CH$_2$–), 121.97 (C5), 124.35 (picrate), 125.10 (picrate), 141.75 (picrate), 144.77 (C4), 145.18 (C2), 160.52 (picrate).

1-Pentyl-2-methyl-4-nitroimidazolium Picrate ([1-Pent-2-Me-4-NO$_2$-3-H-IM][Pic]) (14a). Yellow solid, 95% yield; ^{1}H NMR (360 MHz, [D$_6$] DMSO) δ = 0.86 (t, 3H, –CH$_3$), 1.29 (m, 4H, –CH$_2$–CH$_2$–), 1.71 (p, 2H, –CH$_2$–), 2.35 (s, 3H, C2–CH$_3$), 3.96 (t, 2H, N–CH$_2$–), 8.33 (s, 1H, C5-H), 8.59 (s, 2H, picrate); ^{13}C NMR (90 MHz, [D$_6$] DMSO) δ = 12.51 (–CH$_3$), 13.73 (C2–CH$_3$), 21.57 (–CH$_2$–CH$_3$), 27.67 (–CH$_2$–), 29.12 (–CH$_2$–), 46.32 (N–CH$_2$–), 122.01 (C5), 124.32 (picrate), 125.18 (picrate), 141.76 (picrate), 144.79 (C4), 145.19 (C2), 160.56 (picrate).

1-Hexyl-4-nitroimidazolium Picrate ([1-Hex-4-NO$_2$-3-H-IM][Pic]) (15a). Yellow viscous liquid, 94% yield; ^{1}H NMR (360 MHz, [D$_6$] DMSO) δ = 0.84 (t, 3H, –CH$_3$), 1.25 (m, 6H, –CH$_2$–CH$_2$–CH$_2$–), 1.76 (p, 2H, –CH$_2$–), 4.05 (t, 2H,

N–CH$_2$–), 7.88 (d, 1H, C5-H), 8.44 (s, 1H, C2-H), 8.59 (s, 2H, picrate); ^{13}C NMR (90 MHz, [D$_6$] DMSO) δ = 13.50 (–CH$_3$), 21.51 (–CH$_2$–CH$_3$), 24.93, 29.24, 30.22 (–CH$_2$–), 47.75 (N–CH$_3$–), 119.14 (C5), 124.87 (picrate), 125.18 (picrate), 135.18 (C2), 141.53 (picrate), 144.20 (C4), 160.49 (picrate).

1-Methyl-2,4-dinitroimidazolium Picrate ([1-Me-2,4-diNO$_2$-3-H-IM][Pic]) (16a). This reaction failed. Yellow co-crystals of 1-methyl-2,4-dinitroimidazole and picric acid were isolated, 1-Me-2,4-diNO$_2$-IM·HPic.

1-Methyl-4,5-dinitroimidazolium Picrate ([1-Me-4,5-diNO$_2$-3-H-IM][Pic]) (17a). This reaction failed. No product was observed, only a mixture of the reactants.

1-Methyl-4,5-dicyanoimidazolium Picrate ([1-Me-4,5-diCN-3-H-IM][Pic]) (18a). This reaction failed. Yellow co-crystals of 1-methyl-4,5-dicyanoimidazole and picric acid were isolated, 1-Me-4,5-diCN-IM·1.5 HPic.

1-Methylimidazolium Nitrate ([1-Me-3-H-IM][NO$_3$]) (1b). White solid, 99% yield; ^{1}H NMR (360 MHz, [D$_6$] DMSO) δ = 3.86 (s, 3H, N-CH$_3$), 7.66 (s, 1H, C5-H), 7.69 (s, 1H, C4-H), 9.05 (s, 1H, C2-H); ^{13}C NMR (90 MHz, [D$_6$] DMSO) δ = 35.40 (N–CH$_3$), 119.66, 123.09 (C4/5), 135.86 (C2).

1,2-Dimethylimidazolium Nitrate ([1,2-diMe-3-H-IM][NO$_3$]) (2b). White crystals, 99% yield; ^{1}H NMR (360 MHz, [D$_6$] DMSO) δ = 2.55 (s, 3H, C2-CH$_3$), 3.73 (s, 3H, N–CH$_3$), 7.52 (s, 1H, C5-H), 7.57 (s, 1H, C4-H); ^{13}C NMR (90 MHz, [D$_6$] DMSO) δ = 10.10 (C2-CH$_3$), 33.83 (N–CH$_3$), 117.52, 122.91 (C4/5), 144.41 (C2).

1-Propylimidazolium Nitrate ([1-Pr-3-H-IM][NO$_3$]) (3b). White crystals, 96% yield; ^{1}H NMR (360 MHz, [D$_6$] DMSO) δ = 0.84 (t, 3H, –CH$_3$), 1.81 (m, 2H, –CH$_2$–CH$_3$), 4.15 (t, 3H, N–CH$_2$–), 7.70 (s, 1H, C5-H), 7.90 (s, 1H, C4-H), 9.15 (s, 1H, C2-H); ^{13}C NMR (90 MHz, [D$_6$] DMSO) δ = 10.26 (–CH$_3$), 22.72 (–CH$_2$–CH$_3$), 49.86 (N–CH$_2$–), 119.80, 121.84 (C4/C5), 135.13 (C2).

1-Butylimidazolium Nitrate ([1-Bu-3-H-IM][NO$_3$]) (4b). Colorless liquid, 99% yield; ^{1}H NMR (360 MHz, [D$_6$] DMSO) δ = 0.90 (t, 3H, –CH$_3$), 1.25 (sextet, 2H, –CH$_2$–), 1.80 (p, 2H, –CH$_2$–), 4.21 (t, 2H, N–CH$_2$–), 7.72 (s, 1H, C5-H), 7.82 (s, 1H, C4-H), 9.19 (s, 1H, C2-H); ^{13}C NMR (90 MHz, [D$_6$] DMSO) δ = 13.25, 18.84, 31.45 (alkyl), 48.23 (N–CH$_2$–), 120.08, 122.00 (C4/5), 135.35 (C2).

1-Butyl-2-methylimidazolium Nitrate ([1-Bu-2-Me-3-H-IM][NO$_3$]) (5b). White solid, 97% yield; ^{1}H NMR (360 MHz, [D$_6$] DMSO) δ = 0.90 (t, 3H, –CH$_3$), 1.28 (m, 2H, –CH$_2$–CH$_3$), 1.71 (p, 2H, –CH$_2$–CH$_2$–), 2.58 (s, 3H, C2–CH$_3$), 4.07 (t, 3H, N–CH$_2$–), 7.57 (s, 1H, C5-H), 7.66 (s, 1H, C4-H); ^{13}C NMR (90 MHz, [D$_6$] DMSO) δ = 10.15 (–CH$_3$), 13.33 (C2–CH$_3$), 18.91 (–CH$_2$–CH$_3$), 30.95 (–CH$_2$–), 46.47 (N–CH$_2$–), 117.93, 121.99 (C4/C5), 143.79 (C2).

1-Pentyl-2-methylimidazolium Nitrate ([1-Pent-2-Me-3-H-IM][NO$_3$]) (6b). White solid, 96% yield; ^{1}H NMR (360 MHz, [D$_6$] DMSO) δ = 0.87 (t, 3H, –CH$_3$), 1.30 (m, 4H, –CH$_2$–CH$_2$–), 1.73 (p, 2H, –CH$_2$–CH$_2$–), 2.58 (s, 3H, C2–CH$_3$), 4.07 (t, 3H, N–CH$_2$–), 7.57 (s, 1H, C5-H), 7.66 (s, 1H, C4-H); ^{13}C NMR (90 MHz, [D$_6$] DMSO) δ = 10.16 (–CH$_3$), 13.71 (C2–CH$_3$), 21.55 (–CH$_2$–CH$_3$), 27.73 (–CH$_2$–), 28.63 (–CH$_2$–), 46.67 (N–CH$_2$–), 117.94, 121.78 (C4/C5), 143.79 (C2).

1-Hexylimidazolium Nitrate ([1-Hex-3-H-IM][NO$_3$]) (7b). White solid, 98% yield; ^{1}H NMR (360 MHz, [D$_6$] DMSO) δ = 0.84 (t, 3H, –CH$_3$), 1.25 (m, 6H, –CH$_2$–CH$_2$–CH$_2$–), 1.79 (p, 2H, –CH$_2$–CH$_2$–), 4.18 (t, 3H, N–CH$_2$–), 7.70 (s, 1H, C5-H), 7.81 (s, 1H, C4-H), 9.17 (s, 1H, C2-H); ^{13}C NMR (90 MHz, [D$_6$] DMSO) δ = 13.76 (–CH$_3$), 21.82 (–CH$_2$–CH$_3$), 25.13 (–CH$_2$–), 29.32 (–CH$_2$–), 30.46 (–CH$_2$–), 48.45 (N–CH$_2$–), 119.89, 121.93 (C4/C5), 135.22 (C2).

1-Methyl-2-nitroimidazolium Nitrate ([1-Me-2-NO$_2$-3-H-IM][NO$_3$]) (8b). White solid, 82% yield; ^{1}H NMR (360 MHz, [D$_6$] DMSO) δ = 4.00 (s, 3H, N–CH$_3$), 7.17 (s, 1H, C5-H), 7.65 (s, 1H, C4-H), 11.49 (b, N-H); ^{13}C NMR (90 MHz, [D$_6$] DMSO) δ = 37.07 (N–CH$_3$), 127.49, 128.51 (C4/5), 141.31 (C2).

1,2-Dimethyl-5-nitroimidazolium Nitrate ([1,2-diMe-5-NO$_2$-3-H-IM][NO$_3$]) (9b). White solid, 84% yield; ^{1}H NMR (360 MHz, [D$_6$] DMSO) δ = 2.52 (s, 3H, C2-CH$_3$), 3.87 (s, 3H, N–CH$_3$), 8.36 (s, 1H, C4-H), 12.1 (b, N–H); ^{13}C NMR (90 MHz, [D$_6$] DMSO) δ = 12.81 (C2-CH$_3$), 33.62 (N–CH$_3$), 122.87 (C4), 138.55 (C2), 149.82 (C5).

1-Ethyl-2-nitroimidazolium Nitrate ([1-Et-2-NO$_2$-3-H-IM][NO$_3$]) (10b). Colorless liquid, 85% yield; ^{1}H NMR (360 MHz, [D$_6$] DMSO) δ = 1.38 (t, 3H, –CH$_3$), 4.39 (q, 2H, N–CH$_2$–), 7.17 (d, 1H, C5-H), 7.70 (d, 1H, C4-H); ^{13}C NMR (90 MHz, [D$_6$] DMSO) δ = 15.57 (–CH$_3$), 44.72 (N–CH$_2$), 127.08, 127.88 (C4/5), 149.16 (C2).

1-Ethyl-4-nitroimidazolium Nitrate ([1-Et-4-NO$_2$-3-H-IM][NO$_3$]) (11b). Colorless liquid, 89% yield; ^{1}H NMR (360 MHz, [D$_6$] DMSO) δ = 1.39 (t, 3H, –CH$_3$), 4.08 (q, 2H, N–CH$_2$–), 7.89 (s, 1H, C5-H), 8.46 (s, 1H, C2-H); ^{13}C NMR (90 MHz, [D$_6$] DMSO) δ = 15.70 (–CH$_3$), 42.50 (N–CH$_2$), 121.20 (C5), 136.95 (C2), 145.86 (C4).

1-Isopropyl-4-nitroimidazolium Nitrate ([1-*i*-Pr-4-NO$_2$-3-H-IM][NO$_3$]) (12b). White solid, 89% yield; ^{1}H NMR (360 MHz, [D$_6$] DMSO) δ = 1.44 (d, 6H, –CH$_3$), 4.52 (m, 1H, N–CH–), 7.95 (s, 1H, C5-H), 8.52 (s, 1H, C2-H); ^{13}C NMR (90 MHz, [D$_6$] DMSO) δ = 22.71 (–CH$_3$), 50.33 (N–CH–), 119.64 (C5), 135.75 (C4), 146.93 (C2).

1-Butyl-2-methyl-4-nitroimidazolium Nitrate ([1-Bu-2-Me-4-NO$_2$-3-H-IM][NO$_3$]) (13b). White solid, 93% yield; ^{1}H NMR (360 MHz, [D$_6$] DMSO) δ = 0.90 (t, 3H, –CH$_3$), 1.28 (m, 2H, –CH$_2$–CH$_3$), 1.69 (p, 2H, –CH$_2$–), 2.35 (s, 3H, C2-CH$_3$), 3.97 (t, 2H, N–CH$_2$–), 8.33 (s, 1H, C5-H); ^{13}C NMR (90 MHz, [D$_6$] DMSO) δ = 12.49 (–CH$_3$), 13.32 (C2–CH$_3$), 18.97 (–CH$_2$–CH$_3$), 31.43 (–CH$_2$–), 46.07 (N–CH$_2$–), 122.07 (C5), 144.71 (C4), 145.11 (C2).

1-Pentyl-2-methyl-4-nitroimidazolium Nitrate ([1-Pent-2-Me-4-NO$_2$-3-H-IM][NO$_3$]) (14b). Colorless viscous liquid, 97% yield; ^{1}H NMR (360 MHz, [D$_6$] DMSO) δ = 0.86 (t, 3H, –CH$_3$), 1.30 (m, 4H, –CH$_2$–CH$_2$–), 1.71 (p, 2H, –CH$_2$–), 2.35 (s, 3H, C2–CH$_3$), 3.96 (t, 2H, N–CH$_2$–), 8.34 (s, 1H, C5-H);

^{13}C NMR (90 MHz, [D$_6$] DMSO) δ = 12.28 (–CH$_3$), 13.50 (C2–CH$_3$), 21.33 (–CH$_2$–CH$_3$), 27.63 (–CH$_2$–), 28.88 (–CH$_2$–), 46.07 (N–CH$_2$–), 121.79 (C5), 144.55 (C4), 145.10 (C2).

1-Hexyl-4-nitroimidazolium Nitrate ([1-Hex-4-NO$_2$-3-H-IM][NO$_3$]) (15b). Colorless viscous liquid, 95% yield; ^{1}H NMR (360 MHz, [D$_6$] DMSO) δ = 0.85 (t, 3H, –CH$_3$), 1.25 (m, 6H, –CH$_2$–CH$_2$–CH$_2$–), 1.75 (p, 2H, –CH$_2$–), 4.03 (t, 2H, N–CH$_2$–), 7.85 (d, 1H, C5-H), 8.44 (s, 1H, C2-H); ^{13}C NMR (90 MHz, [D$_6$] DMSO) δ = 13.76 (–CH$_3$), 21.82 (–CH$_2$–CH$_3$), 25.26, 29.79, 30.47 (–CH$_2$–), 47.26 (N–CH$_3$–), 121.44, (C5), 125.10 (C2), 137.29 (C4).

1-Methyl-2,4-dinitroimidazolium Nitrate ([1-Me-2,4-diNO$_2$-3-H-IM][NO$_3$]) (16b). No product was observed, only a mixture of reactants.

1-Methyl-4,5-dinitroimidazolium Nitrate ([1-Me-4,5-diNO$_2$-3-H-IM][NO$_3$]) (17b). No product was observed, only a mixture of reactants.

1-Methyl-4,5-dicyanoimidazolium Nitrate ([1-Me-4,5-diCN-3-H-IM][NO$_3$]) (18b). No product was observed, only a mixture of reactants.

General protocol for the synthesis of alkylated imidazolium salt derivatives

1,3-Dimethylimidazolium chloride (1,3-diMeIM][Cl]) (**19c**) and 1,2,3-trimethylimidazolium chloride ([1,2,3-triMeIM][Cl]) (**20c**) were prepared by purging chloromethane gas through an EtOH solution of either 1-methylimidazole or 1,2-dimethylimidazole at 0 °C similar to a protocol presented in the literature.[54] 1-Butyl-3-methylimidazolium chloride (1-Bu-3-MeIM][Cl]) (**21c**) was prepared using the standard literature protocol by reacting 1-methylimidazole with a 30% excess of chlorobutane at 70 °C and later removal of unreacted substrates under vacuum.[55]

1,3-Dimethylimidazolium nitrate ([1,3-diMeIM][NO$_3$]) (**19b**), 1,2,3-trimethyl imidazolium nitrate ([1,2,3-triMeIM][NO$_3$]) (**20b**), and 1-butyl-3-methylimidazolium nitrate ([1-Bu-3-MeIM][NO$_3$]) (**21b**) were prepared from their chloride precursors by the anion exchange reaction of the chloride salt with silver nitrate (1 : 1 molar ratio) in aqueous solution utilizing a previously reported protocol.[56] Equimolar amounts of silver nitrate, dissolved in water, and imidazolium chloride salt, dissolved in water, were mixed together by dropwise addition of silver nitrate solution into a stirred solution of chloride salt. After the solution was stirred in the dark for 24 h, the silver chloride was removed by filtration, and the filtrate checked for the presence of silver ions using HCl. The solvent was then evaporated at 80 °C under vacuum. A final purification step involved dissolution of the obtained nitrate salt in dry ethanol in order to separate it from any solid, inorganic by-product. The salts were then dried under high vacuum at 60 °C for an additional 5 h.

1,3-Dimethylimidazolium, 1,2,3-trimethylimidazolium, and 1-butyl-3-methylimidazolium picrate salts ware prepared from their chloride precursors by an anion exchange reaction of the chloride salt with sodium picrate (1 : 1 molar ratio) in a mixture of EtOH/H$_2$O. Solvent was evaporated using high vacuum, the samples were re-dissolved in water, and the picrate salts were extracted from the aqueous phase using chloroform. Following this, the salts were dried under high vacuum at 60 °C for an additional 5 h. The possible presence of chloride anions was tested using aqueous solution of silver nitrate.

1,3-Dimethylimidazolium Nitrate ([1,3-diMeIM][NO$_3$]) (19b). White solid, 65% yield; ^{1}H NMR (360 MHz, [D$_6$] DMSO) δ = 3.83 (s, 6H, N-CH$_3$), 7.69 (d, 2H, C4/C5-H), 9.03 (s, 1H, C2-H); ^{13}C NMR (90 MHz, [D$_6$] DMSO) δ = 35.59 (N–CH$_3$), 123.33 (C4/C5), 136.99 (C2).

1,2,3-Trimethylimidazolium Nitrate ([1,2,3-triMeIM][NO$_3$]) (20b). White crystalline solid, 70% yield; ^{1}H NMR (500 MHz, [D$_4$] MeOH) δ = 2.58 (s, 3H, C2–CH$_3$), 3.85 (s, 6H, N–CH$_3$), 7.43 (s, 2H, C4/C5-H); ^{13}C NMR (125 MHz [D$_4$] MeOH) δ = 10.02 (C2–CH$_3$), 35.33 (N–CH$_3$), 123.26 (C4/C5), 146.42 (C2).

1-Butyl-3-methylimidazolium Nitrate ([1-Bu-3-MeIM][NO$_3$]) (21b). Colorless liquid, 69% yield; ^{1}H NMR (500 MHz, [D$_6$] DMSO) δ = 0.91 (t, 3H, –CH$_3$), 1.33 (m, 2H, –CH$_2$–CH$_3$), 1.87 (m, 2H, –CH$_2$–), 4.05 (s, 3H, N–CH$_3$), 4.29 (t, 2H, N–CH$_2$–), 7.59 (s, 1H, C5-H), 7.77 (s, 1H, C4-H), 9.06 (s, 1H, C2-H); ^{13}C NMR (125 MHz [D$_6$] DMSO) δ = 13.45 (–CH$_3$), 20.10 (–CH$_2$–CH$_3$), 32.59 (–CH$_2$–CH$_2$–), 37.00 (N–CH$_3$), 49.93 (N–CH$_2$–), 122.23, 123.87 (C4/C5), 138.67 (C2).

1,3-Dimethylimidazolium Picrate ([1,3-diMeIM][Pic]) (19a). Yellow solid, 78% yield; ^{1}H NMR (360 MHz, [D$_6$] DMSO) δ = 3.82 (s, 6H, N-CH$_3$), 7.68 (d, 2H, C4/C5-H), 8.60 (s, 2H, picrate), 9.02 (s, 1H, C2-H); ^{13}C NMR (90 MHz, [D$_6$] DMSO) δ = 35.58 (*N*-CH$_3$), 123.32 (C4/C5), 124.07 (picrate), 125.10 (picrate), 136.95 (C2), 141.74 (picrate), 160.73 (picrate).

1,2,3-Trimethylimidazolium Picrate ([1,2,3-triMeIM][Pic]) (20a). Yellow crystalline solid, 85% yield; ^{1}H NMR (500 MHz, [D$_4$] MeOH) δ = 2.56 (s, 3H, C2–CH$_3$), 3.75 (s, 6H, N–CH$_3$), 7.59 (s, 2H, C4/C5-H), 8.59 (s, 2H, picrate); ^{13}C NMR (125 MHz [D$_4$] MeOH) δ = 9.47 (C2–CH$_3$), 34.54 (N–CH$_3$), 121.81 (C4/C5), 124.03 (picrate), 125.09 (picrate), 141.70 (picrate), 144.57 (C2), 160.70 (picrate).

1-Butyl-3-methylimidazolium Picrate ([1-Bu-3-MeIM][Pic]) (21a). Yellow viscous liquid, 84% yield; ^{1}H NMR (360 MHz, [D$_6$] DMSO) δ = 0.93 (t, 3H, –CH$_3$), 1.36 (m, 2H, –CH$_2$–CH$_3$), 1.81 (m, 2H, –CH$_2$–), 4.00 (s, 3H, N–CH$_3$), 4.33 (t, 2H, N–CH$_2$–), 7.50 (s, 1H, C5-H), 7.71 (s, 1H, C4-H), 8.57 (s, 2H, picrate), 9.02 (s, 1H, C2-H); ^{13}C NMR (125 MHz [D$_6$] DMSO) δ = 13.22 (–CH$_3$), 20.90 (–CH$_2$–CH$_3$), 33.02 (–CH$_2$–CH$_2$–), 37.28 (N–CH$_3$), 49.15 (N–CH$_2$–), 122.21, 123.65 (C4/C5), 124.15 (picrate), 125.11 (picrate), 138.55 (C2), 141.38 (picrate), 160.76 (picrate).

Conclusion

The focus of this work was on exploring the possibility of forming simple energetic ionic liquids *via* the straightforward protonation of neutral imidazole derivatives with nitric or picric acids. Moreover, the influence of substituent type (nitro-, cyano-, alkyl-substituents) and position on the properties of the resulting protonated imidazolium salts was investigated.

This easy acid–base chemistry approach resulted in the formation of a large family of protonated imidazolium picrate and nitrate salts but was not without limitations. It was found that functionalization of imidazoles with electron-withdrawing substituents such as nitro or cyano resulted in a reduction in nucleophilicity of the heterocycle. Mononitro-substituted protonated imidazolium salts could be isolated, but further ring substitution with electron-withdrawing groups resulted in the imidazoles failing to undergo protonation even with a strong acid such as HCl. The only products that were obtained were co-crystals of 1-Me-4,5-diCN-IM and 1-Me-2,4-diNO_2-IM with picric acid.

The melting points of the protonated salts were much lower than expected, and from the group of 30 analyzed compounds, more than half were found to melt below 100 °C. General trends in the melting points of the analyzed salts show that melting transitions of picrate-based salts were always higher than that of their nitrate analogs. Additionally, analysis of the melting point variations as a function of the *N*-alkyl chain length shows that the longer the alkyl chain, the lower the melting point of the resulting salt until the alkyl chain extends over four carbons, at which point an increase of the melting point was observed. It was also found that 1,2-dialkyl-substituted salts generally melted at higher temperatures than those not possessing a methyl substituent on the C2 carbon in the ring. Comparing the influence of the position of the $–NO_2$ group on the melting point of the salts using two isomeric compounds, it was found that the melting point does not change greatly. On the other hand, this structural change significantly influenced the thermal stability of the two isomers, and by changing the position of the $–NO_2$ group from C2 to C4 resulted in an increase in stability for both nitrates and picrates.

Analysis of the thermal stabilities of the salts revealed that all $[NO_3]^-$-based salts are less stable than their $[Pic]^-$ analogs. Typically, the difference between the thermal stabilities of nitrate and picrate salts was *ca.* 50 °C. Moreover, it was found that C2-Me-substituted picrate salts tended to be more stable than those which are unsubstituted, unfortunately at the same time exhibited higher melting points. It was found that the decomposition temperatures for the nitrate and picrate salts substituted with $–NO_2$ groups seem to be *ca.* 20–50 °C lower than those that were not nitro-substituted. It was concluded that the thermal stability range for each group of salts is more dependent on the structure of the anion than on the presence of the substituents on C2 carbon position or the alkyl chain length of the *N*-alkyl substituents.

Comparing the simple protonated imidazolium nitrate and picrate salts with their methylated analogs, it was found that the protonated ionic liquids did not differ substantially in their melting points from the methylated analogs. However, the thermal stabilities of protonated imidazolium salts were much lower than their alkylated derivatives. Nitrate salts with alkylated cations tended to be more thermally stable than the corresponding picrate salts, but for protonated cations, the picrate salts tended to be approximately 70–80 °C more stable than the nitrate salts.

The decomposition temperatures determined by accelerating rate calorimetry experiments under oxygen atmosphere roughly corresponded with those found by TGA. The ARC experiments revealed that the alkylated salts were much less explosive than the protonated analogs, and that among all the analyzed salts, the most energetic materials investigated were protonated [1-Me-3-H-IM][NO_3] (**1b**) and [1,2-diMe-3-H-IM][Pic] (**2a**) salts.

Notes and references

1 A. C. Angell, N. Byrne and J. P. Belieres, *Acc. Chem. Res.*, 2007, **40**, 1228.
2 T. L. Greaves and C. J. Drummond, *Chem. Rev.*, 2008, **108**, 206.
3 S. Gabriel, *Berichte*, 1888, **21**, 2664.
4 P. Walden, *Bull. Acad. Sci. St. Petersburg*, 1914, 405.
5 J. Pernak, I. Goc and I. Mirska, *Green Chem.*, 2004, **6**, 323.
6 J. Pernak, I. Goc and A. Fojutowski, *Holzforschung*, 2005, **59**, 473.
7 Y. Gu, F. Shi and Y. Deng, *Catal. Commun.*, 2003, **4**, 597.
8 A. Cole, J. Jensen, I. Ntai, K. Tran, K. Weaver, D. Forbes and J. Davis, *J. Am. Chem. Soc.*, 2002, **124**, 5962.
9 Y. Gu, F. Shi and Y. Deng, *J. Mol. Catal. A: Chem.*, 2004, **212**, 71.
10 K. Qiao and C. Yokoyama, *Chem. Lett.*, 2004, **33**, 472.
11 T. Jiang, H. X. Gao, B. X. Han, G. Y. Zhao, Y. H. Chang, W. Z. Wu, L. Gao and G. Yang, *Tetrahedron Lett.*, 2004, **45**, 2699.
12 V. K. Aggarwal, C. Lopin and F. Sandrinelli, *J. Am. Chem. Soc.*, 2003, **125**, 7596.
13 M. Picquet, I. Tkatchenko, I. Tommasi, P. Wasserscheid and J. Zimmermann, *Adv. Synth. Catal.*, 2003, **345**, 959.
14 C. F. Poole, *J. Chromatogr., A*, 2004, **1037**, 49.
15 A. Noda, M. Susan, K. Kudo, S. Mitsushima, K. Hayamizu and M. Watanabe, *J. Phys. Chem. B*, 2003, **107**, 4024.
16 A. B. H. Susan, A. Noda, S. Mitsushima and M. Watanabe, *Chem. Commun.*, 2003, 938.
17 H. Nakamoto, A. Noda, K. Hayamizu, S. Hayashi, H. Hamaguchi and M. Watanabe, *J. Phys. Chem. C*, 2007, **111**, 1541.
18 D. F. Evans, *Langmuir*, 1988, **4**, 3.
19 R. Atkin and G. G. Warr, *J. Am. Chem. Soc.*, 2005, **127**, 11940.
20 T. L. Greaves, A. Weerawardena, C. Fong and C. J. Drummond, *J. Phys. Chem. B*, 2007, **111**, 4082.
21 W. L. Hough, M. Smiglak, H. Rodríguez, R. P. Swatloski, S. K. Spear, D. T. Daly, J. Pernak, J. E. Grisel, R. D. Carliss, M. D. Soutullo, J. H. Davis Jr. and R. D. Rogers, *New J. Chem.*, 2007, **31**, 1429.
22 W. L. Hough and R. D. Rogers, *Bull. Chem. Soc. Jpn.*, 2007, **80**, 2262.
23 J. Stoimenovski, D. R. MacFarlane, K. Bica and R. D. Rogers, *Pharm. Res.*, 2010, **27**, 521.
24 J. C. Galvez-Ruiz, G. Holl, K. Karaghiosoff, T. M. Klapoetke, K. Loehnwitz, P. Mayer, H. Noeth, K. Polborn, C. J. Rohbogner, M. Suter and J. J. Weigand, *Inorg. Chem.*, 2005, **44**, 4237.
25 T. Hawkins, L. Hall, K. Tollison, A. Brand, M. McKay and G. W. Drake, *Propellants, Explos., Pyrotech.*, 2006, **31**, 196.
26 H. Gao, C. Ye, O. D. Gupta, J. C. Xiao, M. A. Hiskey, B. Twamley and J. M. Shreeve, *Chem.–Eur. J.*, 2007, **13**, 3853.
27 T. L. Greaves and C. J. Drummond, *Chem. Rev.*, 2008, **108**, 206.
28 M. Hirao, H. Sugimoto and H. Ohno, *J. Electrochem. Soc.*, 2000, **147**, 4168.
29 T. L. Greaves, A. Weerawardena, C. Fong, I. Krodkiewska and C. J. Drummond, *J. Phys. Chem. B*, 2006, **110**, 22479.
30 H. Luo, J. F. Huang and S. Dai, *Sep. Sci. Technol.*, 2008, **43**, 2473.
31 H. Luo, G. A. Baker, J. S. Lee, R. M. Pagni and S. Dai, *J. Phys. Chem. B*, 2009, **113**, 4181.
32 M. Anouti, M. Caillon-Caravanier, C. Le Floch and D. Lemordant, *J. Phys. Chem. B*, 2008, **112**, 9406.
33 M. Anouti, M. Caillon-Caravanier, Y. Dridi, H. Galiano and D. Lemordant, *J. Phys. Chem. B*, 2008, **112**, 13335.
34 J. C. Bryan, M. N. Burnett and A. A. Gakh, *Acta Crystallogr., Sect. C: Cryst. Struct. Commun.*, 1998, **54**, 1229.
35 M. A. Petrie, J. A. Sheehy, J. A. Boatz, G. Rasul, G. K. S. Prakash, G. A. Olah and K. O. Christe, *J. Am. Chem. Soc.*, 1997, **119**, 8802.
36 W. Fraenk, H. Noeth, T. M. Klapoetke and M. Suter, *Z. Naturforsch., B: Chem. Sci.*, 2002, **57**, 621.
37 J. Belieres and C. A. Angell, *J. Phys. Chem. B*, 2007, **111**, 492.
38 D. R. MacFarlane and K. R. Seddon, *Aust. J. Chem.*, 2007, **60**, 3.
39 S. Lee, A. Ogawa, M. Kanno, H. Nakamoto, T. Yasuda and M. Watanabe, *J. Am. Chem. Soc.*, 2010, **132**, 9764.

40 K. Bica, J. Shamshina, W. L. Hough, D. R. MacFarlane and R. D. Rogers, *Chem. Commun.*, 2011, **47**, 2267.
41 A. R. Katritzky, H. Yang, D. Zhang, K. Kirichenko, M. Smiglak, J. D. Holbrey, W. M. Reichert and R. D. Rogers, *New J. Chem.*, 2006, **30**, 349.
42 K. E. Gutowski, J. D. Holbrey, R. D. Rogers and D. A. Dixon, *J. Phys. Chem. B*, 2005, **109**, 23196.
43 J. D. Holbrey and R. D. Rogers, Physicochemical Properties: Physicochemical Properties of Ionic Liquids: Melting Points and Phase Diagrams, in *Ionic Liquids in Synthesis*, (2nd edn), ed. P. Wasserscheid and T. Welton, Wiley-VCH Verlag GmbH & Co. KgaA, Weinheim, Germany, 2008, pp. 57–72.
44 J. L. Anthony, J. F. Brennecke, J. D. Holbrey, E. J. Maginn, R. A. Mantz, R. D. Rogers, P. C. Trulove, A. E. Visser and T. Welton, Physicochemical Properties of Ionic Liquids, in *Ionic Liquids in Synthesis*, ed. P. Wasserscheid and T. Welton, Wiley-VCH Verlag GmbH & Co. KgaA, Weinheim, Germany, 2003, pp. 41–55.
45 J. Sarasin, *Helv. Chim. Acta*, 1923, **3**, 370.
46 H. Ohno and M. Yoshizawa, *Solid State Ionics*, 2002, **154–155**, 303.
47 N. Sawa, *Nippon Kagaku Zassi*, 1968, **89**, 868.
48 SAINT + NT, version 6.45, Bruker-AXS: Madison, WI, 2003.
49 G. M. Sheldrick, *Acta Crystallogr., Sect. A: Found. Crystallogr.*, 2007, **64**, 112.
50 L. Sun, A. Waterfeld and J. S. Thrasher, *J. Fluorine Chem.*, 2006, **127**, 1436.
51 C. G. Begg, M. R. Grimmett and P. D. Wethey, *Aust. J. Chem.*, 1973, **26**, 2435.
52 B. Lenarcik and P. Ojczenasz, *J. Heterocycl. Chem.*, 2002, **39**, 287.
53 H. Ohno, M. Yoshizawa and W. Ogihara, *Electrochim. Acta*, 2004, **50**, 255.
54 Z. Szulc and J. Mlochowski, *Pol. J. Chem.*, 1986, **60**, 615.
55 J. G. Huddleston, A. E. Visser, W. M. Reichert, H. D. Willauer, G. A. Broker and R. D. Rogers, *Green Chem.*, 2001, **3**, 156.
56 L. Cammarata, S. G. Kazarian, P. A. Salter and T. Welton, *Phys. Chem. Chem. Phys.*, 2001, **3**, 5192.

